Cell Reports

Article

# Physiological shedding and C-terminal proteolytic processing of TMEM106B

## Graphical abstract

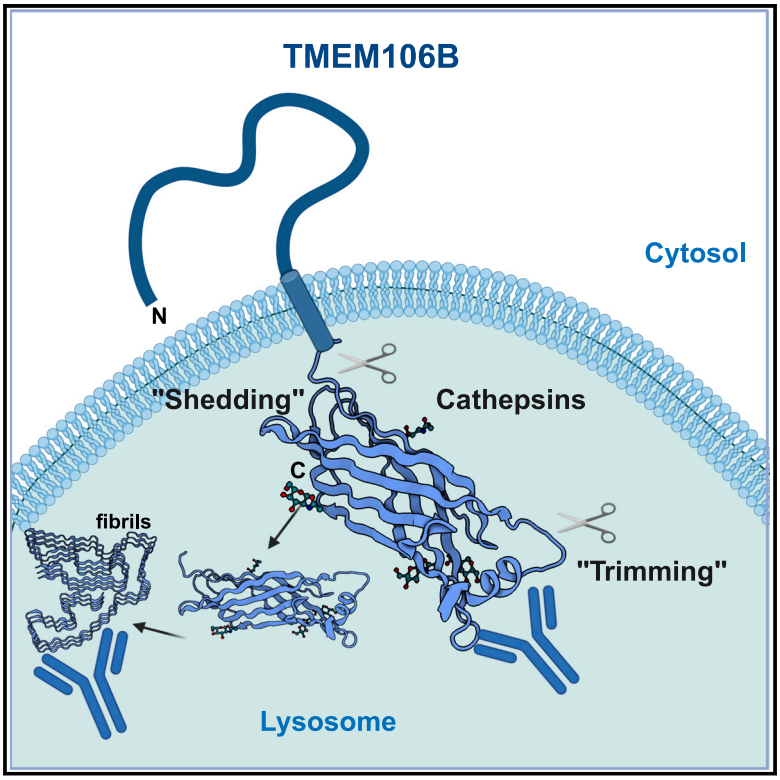


## Authors

Sebastian Held, Christian Erck, Susanna Kemppainen, ..., Patrick Lüningschrör, Anja Capell, Markus Damme

## Correspondence

mdamme@biochem.uni-kiel.de

## In brief

TMEM106B is a lysosomal type II transmembrane protein of unknown function that can form fibrils upon proteolysis. Held et al. show that the luminal domain is generated under physiological conditions by lysosomal cathepsin proteases and that additional proteolysis occurs at the C terminus of TMEM106B.

## Highlights

- The TMEM106B luminal domain is generated under physiological conditions
- The luminal domain of TMEM106B undergoes proteolysis at the C terminus
- The luminal domain of TMEM106B can be detected in iPSC neurons and human and mouse brains

Held et al., 2025, Cell Reports *44*, 115107
January 28, 2025 
https://doi.org/10.1016/j.celrep.2024.115107

CellPress

Cell Reports

CellPress
OPEN ACCESS

Article

# Physiological shedding and C-terminal proteolytic processing of TMEM106B

Sebastian Held,[1] Christian Erck,[2,3] Susanna Kemppainen,[4] Florian Bleibaum,[1] Neha Jadhav Giridhar,[5] Regina Feederle,[6,7,8] Claudia Krenner,[9] Sini-Pauliina Juopperi,[4] Anna Calliari,[10] Torben Mentrup,[11] Bernd Schröder,[11] Dennis W. Dickson,[10,12] Tuomas Rauramaa,[13,14] Leonard Petrucelli,[10,12] Mercedes Prudencio,[10,12] Mikko Hiltunen,[4] Patrick Lüningschrör,[5] Anja Capell,[8,9] and Markus Damme[1,15,*]

[1]Institute of Biochemistry, Christian-Albrechts-University Kiel, Olshausenstrasse 40, 24118 Kiel, Germany
[2]Cellular Proteome Research, Helmholtz Centre for Infection Research, 38124 Braunschweig, Germany
[3]Synaptic Systems GmbH, Rudolf-Wissell-Straβe 28a, 37079 Göttingen, Germany
[4]Institute of Biomedicine, University of Eastern Finland, Kuopio, Finland
[5]Institute of Clinical Neurobiology, University Hospital Würzburg, Versbacher Str. 5, 97078 Würzburg, Germany
[6]Monoclonal Antibody Core Facility, German Research Center for Environmental Health, Neuherberg, Germany
[7]Munich Center for Systems Neurology (SyNergy), Munich, Germany
[8]German Center for Neurodegenerative Diseases (DZNE) Munich, Munich, Germany
[9]Division of Metabolic Biochemistry, Biomedical Center (BMC), Faculty of Medicine, Ludwig-Maximilians-Universität München, Munich, Germany
[10]Department of Neuroscience, Mayo Clinic, Jacksonville, FL 32224, USA
[11]Institute of Physiological Chemistry, Medizinische Fakultät und Universitätsklinikum Carl Gustav Carus, Technische Universität Dresden, 01307 Dresden, Germany
[12]Neurobiology of Disease Graduate Program, Mayo Graduate School, Mayo Clinic College of Medicine, Rochester, MN 55905, USA
[13]Department of Clinical Pathology, Kuopio University Hospital, Kuopio, Finland
[14]Unit of Pathology, Institute of Clinical Medicine, University of Eastern Finland, Kuopio, Finland
[15]Lead contact
*Correspondence: mdamme@biochem.uni-kiel.de
https://doi.org/10.1016/j.celrep.2024.115107

## SUMMARY

Genetic variants in *TMEM106B*, coding for a transmembrane protein of unknown function, have been identified as critical genetic modulators in various neurodegenerative diseases with a strong effect in patients with frontotemporal degeneration. The luminal domain of TMEM106B can form amyloid-like fibrils upon proteolysis. Whether this luminal domain is generated under physiological conditions and which protease(s) are involved in shedding remain unclear. We developed a commercially available antibody against the luminal domain of TMEM106B, allowing a detailed survey of the proteolytic processing under physiological conditions in cellular models and TMEM106B-related mouse models. Moreover, fibrillary TMEM106B was detected in human autopsy material. We find that the luminal domain is generated by multiple lysosomal cysteine-type proteases. Cysteine-type proteases perform additional C-terminal trimming, for which experimental evidence has been lacking. The presented results allow an in-depth perception of the processing of TMEM106B, a prerequisite to understanding factors leading to fibril formation.

## INTRODUCTION

The dysfunction of lysosomes as organelles for the catabolic turnover of macromolecules, including proteins and protein aggregates, has been recognized as a critical component in various neurodegenerative diseases.[1,2] Furthermore, current genetics have identified numerous genes coding for lysosomal proteins whose dysfunction directly causes neurodegenerative diseases or modulates disease risk.[1] Genome-wide association studies have identified single-nucleotide polymorphisms (SNPs) in *TMEM106B* (coding for a lysosomal membrane protein) as a critical disease modifier in frontotemporal lobar degeneration (FTLD).[3–6] This effect is most pronounced in patients with heterozygote *GRN* mutations (leading to progranulin haploinsufficiency): in these patients, *TMEM106B* SNPs, including the coding variant (rs3173615; p.T185S), are protective and reduce the risk of developing disease. Moreover, genetic variants in *TMEM106B* were additionally identified as genetic risk factors for chronic traumatic encephalopathy,[7] hippocampal sclerosis,[8,9] limbic-predominant age-related TDP-43 encephalopathy,[9] and, more recently, Alzheimer's disease.[10] Besides modulating disease risk in more common age-related dementias, a dominant mutation in *TMEM106B* is a monogenic cause for a rare form of hypomyelinating leukodystrophy.[11] How genetic variants in a single gene can modulate such a variety of different diseases remains elusive.

TMEM106B is a type II transmembrane protein localized in the membrane of late endosomes and lysosomes,[12] and its

physiological function is currently unknown. It contains a 96 amino acid (aa)-long amino (N)-terminal cytoplasmic tail with no predicted secondary structure, an integral transmembrane segment (aa 97–117), and a carboxy (C)-terminal luminal domain (aa 118–274) that contains five predicted N-glycosylation sites that are all occupied by complex and high-mannose-type N-glycans.[12] The crystal structure of the luminal domain was solved and revealed a compact fibronectin type III domain, a ubiquitous 7-bladed β sandwich fold closely related to immunoglobulin domains.[13] This fibronectin fold is very common, and its function cannot be directly predicted from the crystal structure. However, the structure closely resembles late embryogenesis abundant-2 (LEA-2) proteins, which play a role in plant desiccation tolerance and might function as lipid transfer proteins.[14]

TMEM106B was previously shown to undergo proteolysis upon overexpression, generating an N-terminal fragment, which is a substrate for intramembrane proteolysis upon co-overexpression of the intramembrane protease SPPL2A.[15] However, evidence for the generation of the luminal domain was indirect, and experimental evidence for the luminal domain or its turnover could not be provided.[15]

A breakthrough in TMEM106B-related research was recently achieved when independent studies showed that the C-terminal luminal domain of TMEM106B can form amyloid-like fibrils in the brains of patients with tauopathies, synucleinopathies, β-amyloidoses, progressive supranuclear palsy, and TDP-43 proteinopathies (FTLD-TDP) as well as elderly individuals without a diagnosis of neurodegenerative disease by cryo-electron microscopy (cryo-EM).[16–18] However, whether the fibrils are causative by modulating the genetic disease risk or merely bystanders or modulators to the disease remains to be elucidated. TMEM106B fibrils were found in three different folds that all had in common that they covered part of the luminal domain starting with serine 120 (which is buried within the filament core), they contained four N-glycans, and the very C-terminal aa of the fibril core was glycine 254. Whether the last C-terminal 20 aa were cleaved off or disordered and flexible and therefore not resolved by cryo-EM remained unclear.[16–18]

Besides its central disease-modulating function in neurodegenerative diseases, TMEM106B was identified as a critical host factor in SARS-CoV-2 infection.[19–21] Independent genome-wide CRISPR-Cas9 knockout (KO) screens identified *TMEM106B* as an essential host gene for infection, at least in a subset of cell lines. Later, TMEM106B was identified as a receptor mediating ACE2-independent SARS-CoV-2 cell entry.[13] By employing cryo-EM, the luminal domain of TMEM106B was shown to engage the receptor-binding motif of the SARS-CoV-2 spike protein, thereby allowing cell entry independently of ACE2.[1]

Together, these findings highlight the importance of TMEM106B, particularly in disease conditions, and the need to comprehensively understand the biosynthesis, proteolytic processing/maturation, and function both under physiological and pathophysiological conditions like neurodegenerative diseases and aging or SARS-CoV-2 infections.

So far, many critical questions regarding TMEM106B biology remain unanswered: is the proteolysis of the luminal domain a physiological process? Which protease(s) are endogenous sheddases (i.e., proteases that release the luminal domain)? Where does proteolysis occur? Is proteolysis affected by the variants in *TMEM106B*? Is the lack of the last ~20 aa in the fibrils due to additional C-terminal proteolysis? The lack of antibodies detecting the luminal domain made it difficult to answer most of these questions. Here, we introduce a commercially available monoclonal antibody against the luminal domain of TMEM106B that allows a comprehensive analysis of the biosynthetic and proteolytic steps and the detection of fibrillary TMEM106B. We found that the formation of the luminal domain is a physiological process in mice and human cells, identified lysosomal cysteine-type cathepsin proteases as physiological sheddases, and found no evidence of an involvement of SPPL2A in the proteolysis of TMEM106B. Genetic variants like the "protective SNP" in *TMEM106B* did not affect the generation of the luminal domain, but interestingly, TMEM106B shows a different processing pattern in the brains of *Grn* KO mice (but not haploinsufficient human *GRN* carriers), suggesting an interesting direct link between these two genetic FTLD risk factors. The antibody detects the physiological luminal domain in human autopsy brain tissues and, moreover, detects fibrillary TMEM106B by immunoblot and immunohistochemistry.

## RESULTS

### The luminal domain of TMEM106B is generated under physiological conditions

In the course of extensive testing of commercially available antibodies against the luminal domain of TMEM106B (Figure 1A), we identified a monoclonal antibody (Synaptic Systems, clone #SY-118C4) that specifically detects human and mouse TMEM106B at the endogenous level. Immunoblot analyses of wild-type and *TMEM106B* KO HeLa cell lysates and wild-type and *Tmem106b* KO mouse brain lysates revealed the detection of the full-length protein at ~40 kDa as two bands migrating close to each other. Both bands are absent in the corresponding KO lysates (Figure 1B). Moreover, a diffuse band corresponding to the luminal domain was detected around 25 kDa (mouse brain), in line with the extensive N-glycosylation and possibly additional posttranslational modification(s), like further proteolytic trimming. These data indicate that the luminal domain is generated under physiological conditions to a significant amount (assuming the monoclonal antibody recognizes both the full-length protein and luminal domain with comparable affinities). The luminal domain was detected at a slightly higher molecular weight in HeLa cells as a rather sharp double band at ~25–35 kDa (Figure 1B). It was also detected in all tested peripheral mouse tissues, with slight molecular weight differences between tissues (Figure S1A). Analysis of brain lysates from mice of different ages revealed no major changes in the ratio between the full-length protein and the luminal domain (Figure S1B). Ectopic expression of the mouse or human TMEM106B cDNA in *TMEM106B* KO HeLa cells showed similar detection of TMEM106B of both species, which is expected due to the high similarity of the immunization peptide and the overall high degree of conservation (Figure 1C). Notably, the molecular weight of the luminal domain was comparable, suggesting that the difference observed between HeLa cells and the mouse brain (Figure 1B) is not due to differences in the TMEM106B sequence but the cellular context. We used density-gradient-based subcellular fractionation of the mouse

CellPress
OPEN ACCESS

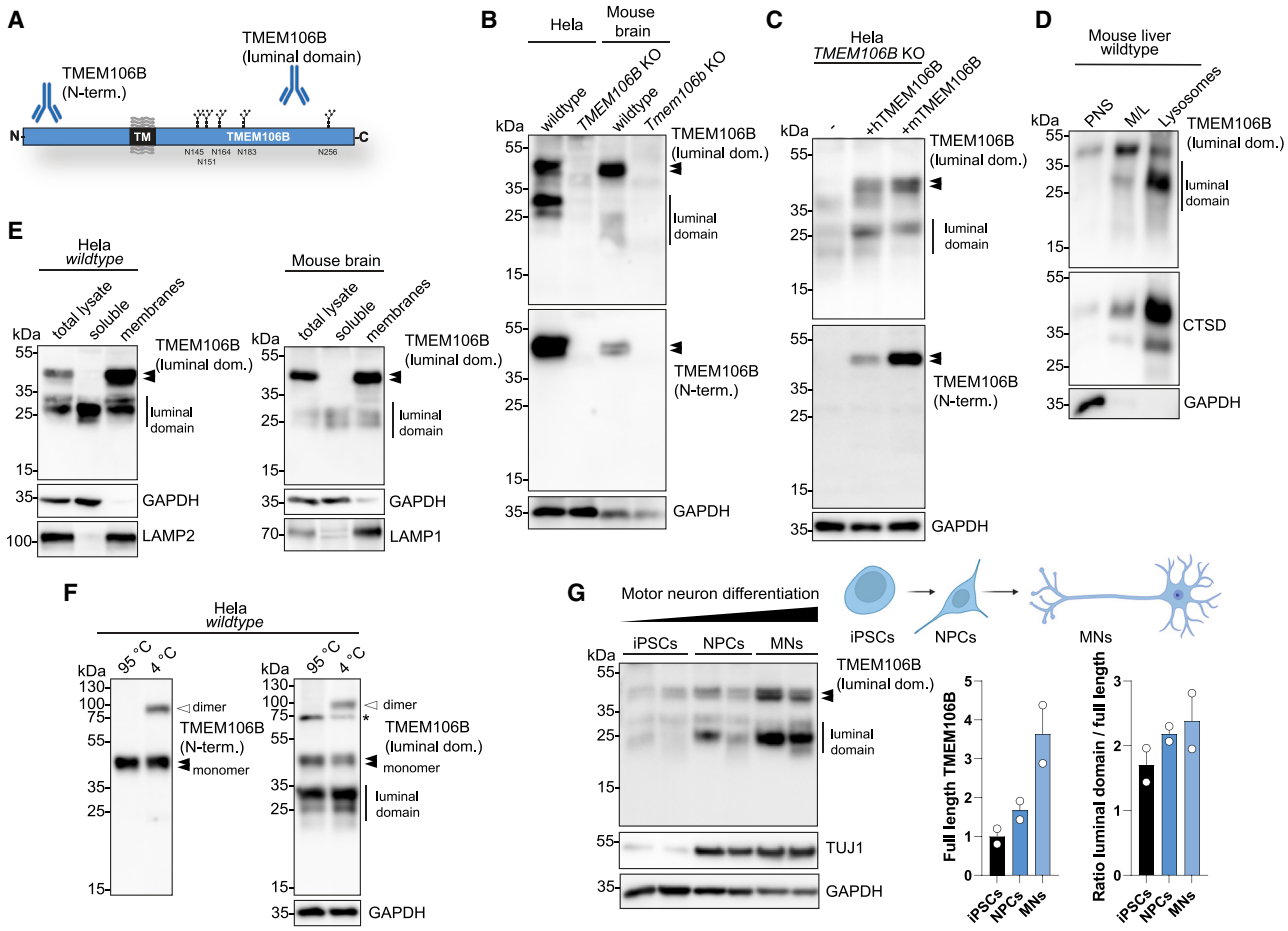


**Figure 1. The luminal domain of TMEM106B is generated under physiological conditions**

(A) Schematic representation of the topology of TMEM106B. The epitope regions of the antibodies against the cytoplasmic N terminus and the luminal domain (epitope: residues 239–252 of human TMEM106B, clone #118C4) are indicated.

(B) Immunoblot analysis of lysates of wild-type and *TMEM106B* KO HeLa cells and wild-type and *Tmem106b* KO mouse brains with the indicated TMEM106B-specific antibodies. GAPDH is shown as a loading control. The double band corresponding to full-length TMEM106B is marked with two arrowheads.

(C) Immunoblot of lysates from untransfected *TMEM106B* KO HeLa cells and cells transfected with plasmids coding for untagged human (hTMEM106B) and murine (mTMEM106B) TMEM106B.

(D) Immunoblot of fractions from lysosome enrichment of the mouse liver (PNS, postnuclear supernatant; M/L, mitochondria+lysosomes enriched) with antibodies against the luminal domain of TMEM106B, CTSD, and GAPDH.

(E) Immunoblot of fractions (total lysates, soluble proteins, membrane proteins) from ultracentrifugation-based membrane separation (cell lysis followed by 100,000 × *g* ultracentrifugation) of wild-type HeLa cells (left) and wild-type mouse brain (right) with antibodies against the luminal domain of TMEM106B, GAPDH as a soluble protein, and LAMP2 (left) or LAMP1 (right) as an integral transmembrane proteins.

(F) Immunoblot analysis of lysates from wild-type HeLa cells with antibodies against the N terminus of TMEM106B (left) or the luminal domain (right). Lämmli lysates were denatured at 95°C or 4°C (as indicated) to detect the putative TMEM106B dimer. GAPDH is depicted as a loading control. * denotes an unspecific band.

(G) Immunoblot analysis of two technical replicates of iPSCs differentiated to NPCs and MNs with antibodies against the luminal domain of TMEM106B. TUJ1 and GAPDH are shown as differentiation markers and a loading control, respectively. Quantifications of the signal intensity of the TMEM106B luminal domain and the ratio between full-length TMEM106B/TMEM106B luminal domain are depicted.

liver and analyzed the different fractions (postnuclear supernatant [PNS], mitochondria+lysosome enriched [ML], lysosome-enriched fractions) with the antibody against the TMEM106B luminal domain (Figure 1D). Notably, in lysosomes, the luminal domain was detected much stronger than the full-length protein, suggesting that a high proportion of TMEM106B undergoes shedding and that the luminal domain is the predominant form in lysosomes.

After shedding, the luminal domain does not contain a transmembrane segment and is presumed to be soluble. To test this experimentally, we applied ultracentrifugation-based membrane fractionation of detergent-free homogenates of HeLa cell lysates and mouse brain lysates to separate membrane-bound and soluble proteins (Figure 1E). Immunoblotting with antibodies against GAPDH, as a marker for soluble proteins, and LAMP1/LAMP2 for integral transmembrane proteins, validated the separation of

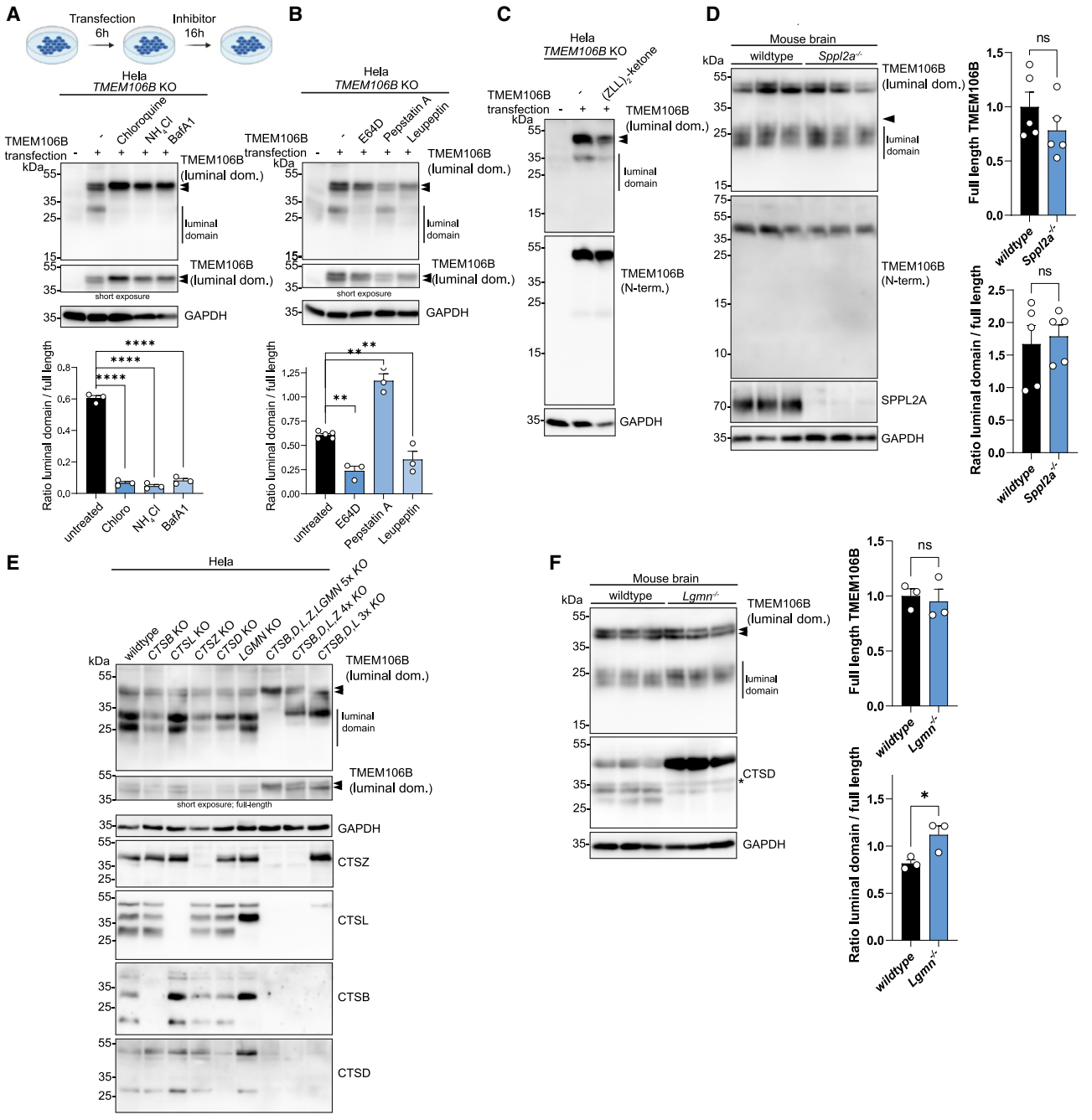


**Figure 2. Proteolytic processing and shedding depend on lysosomal acidification and cysteine-type lysosomal proteases but not SPPL2A**

(A and B) Immunoblot analysis of lysates of wild-type and *TMEM106B* KO HeLa cells re-transfected with wildtype TMEM106B and treated with inhibitors for lysosomal acidification (Chloroquine, Bafilomycin A1, $NH_4Cl$) (A) or with different protease inhibitors (E64D, pepstatin A, leupeptin) (B) with an antibody against the luminal domain of TMEM106B. The (full-length) double band is shown for the with a shorter exposure time. GAPDH is shown as a loading control. Quantification of the signal intensity of the luminal domain/full-length protein ratio is depicted. Data are means ± SEM. Two-tailed unpaired Student's t tests: $^{**}p \leq 0.01$ and $^{****}p \leq 0.0001$.

(C) Immunoblot analysis of lysates of wild-type and *TMEM106B* KO HeLa cells re-transfected with wild-type TMEM106B and treated with $(Z\text{-}LL)_2$ ketone (40 μM), an inhibitor for SPP/SPPL proteases.

(D) Immunoblot analysis of lysates of wild-type *Sppl2a* KO mouse brains with the TMEM106B-specific antibodies. SPPL2A immunoblot is shown for KO validation. GAPDH is shown as a loading control. A quantification of the signal intensity of the luminal domain/full-length protein ratio is depicted. Data are means ± SEM. Two-tailed unpaired Student's t tests: ns $p > 0.05$.

*(legend continued on next page)*

membranes and soluble proteins. Full-length TMEM106B was quantitatively recovered in the membrane fractions, as expected. Surprisingly, the luminal domain was only partially in the soluble protein fraction but significant amounts were still detected in the membrane fraction. This might be suggestive of interactions with membranes, e.g., in the form of homo- or heterodimers with membrane-bound TMEM106B or TMEM106C[22,23] or other membrane interactions (Figure 1E). Which domains of TMEM106B (N terminus, transmembrane, or luminal domain) dimerize remains unknown. To experimentally test if the released luminal domain (lacking the N terminus and the transmembrane segment) alone dimerizes, we tested conditions under which an SDS-resistant TMEM106B dimer is detectable[23] at ~75 kDa (Figure 1F). While the dimer was robustly detectable with both antibodies against the N terminus and the luminal domain, and the (monomeric) luminal domain was detectable, no additional TMEM106B-specific band (corresponding to a putative dimer of the luminal domain) appeared, suggesting that only the full-length protein, but not the luminal domain, forms SDS-resistant dimers. The data suggest that the transmembrane segment or the cytoplasmic N terminus facilitates the dimerization. Finally, we analyzed the proteolytic processing of TMEM106B in a more relevant cell type and differentiated human induced pluripotent stem cells (iPSCs) to neural progenitor cells (NPCs) and differentiated motor neurons (MNs) and analyzed lysates by immunoblot (Figure 1G). While the levels of full-length TMEM106B increased ~3.5-fold over the differentiation to MNs, we observed substantial amounts of the luminal domain, suggesting that TMEM106B proteolysis is of major relevance in neurons. The ratio between the full-length protein and the luminal domain changed only marginally. We conclude that TMEM106B shedding occurs to a significant degree under physiologic conditions in human neurons.

## Lysosomal cysteine-type proteases, but not SPPL2A, are physiological TMEM106B sheddases

Next, we analyzed the effect of pharmacological treatments leading to reduced lysosomal acidification (chloroquine, $NH_4Cl$, Bafilomycin A1 [BafA1]) on the proteolytic processing of TMEM106B. *TMEM106B* KO HeLa cells were transfected with a plasmid coding for untagged TMEM106B in the absence or under conditions of the inhibitor treatment, harvested, and analyzed by immunoblot (Figure 2A). While the luminal domain was robustly detected in untreated cells, the proteolysis was nearly completely inhibited upon treatment with all three drugs. Notably, the double band at ~42/44 kDa shifted entirely to the upper 44 kDa band, suggesting the inhibition of an additional proteolytic event, like C-terminal trimming. In a similar experimental setup, we tested different protease inhibitors (E64D, pepstatin A, leupeptin) regarding their effect on TMEM106B processing (Figure 2B). E64D is a membrane-permeable cysteine-type protease inhibitor; pepstatin A inhibits aspartic proteases, and leupeptin inhibits serin- and cysteine-type proteases. While E64D and leupeptin efficiently inhibited the formation of the luminal domain, pepstatin A had no such effect. Only leupeptin inhibited the formation of the luminal domain plus partially the conversion of the double band toward the upper band, suggesting that cysteine-type protease(s) are critical for the release of the luminal domain (shedding) and additional non-E64D-inhibitable protease(s) contribute to the conversion of the 44 kDa to the 42 kDa band.

SPPL2A was previously shown to degrade an N-terminal fragment of TMEM106B,[15] and more recently, SPPL2A has proven to act as a non-canonical sheddase for the transmembrane protein substrate tumor necrosis factor alpha (TNF-$\alpha$),[24] making it a prime candidate for TMEM106B shedding. To analyze the contribution of SPPL2A to TMEM106B processing, we treated cells with the peptide-based SPPL/SPPL-type protease inhibitor $(Z\text{-}LL)_2$ ketone.[25] Newly, under inhibitor conditions synthesized, re-transfected TMEM106B in *TMEM106B* HeLa KO cells was analyzed by immunoblot (Figure 2C). $(Z\text{-}LL)_2$ ketone treatment did not affect the shedding of TMEM106B, nor did we observe the accumulation of N-terminal fragments as described before.[15] In an independent experimental setup monitoring endogenous TMEM106B, we analyzed brain lysates from *Sppl2a* KO[25] and age-matched wild-type mice with antibodies against the luminal domain and the N terminus of TMEM106B by immunoblot (Figure 2D). No differences could be observed between the two experimental cohorts regarding the formation of the luminal domain, and even more critically, no N-terminal fragment resulting from impaired intramembrane proteolysis could be detected, suggesting that SPPL2A does not play a relevant role in the physiological proteolytic processing of TMEM106B, neither by unconventional shedding nor the degradation of N-terminal fragments. *Sppl2a/b* double-KO mice[26] similarly showed no accumulation of an N-terminal fragment and only a modest decrease in the luminal domain (Figure S2), excluding that SPPL2B can functionally compensate for the loss of SPPL2A. These data, in summary, suggest that SPPL2A/B play only a very minor role in the shedding of TMEM106B, if any at all.

Given the lack of a major effect of SPPL2A/SPPL2B deficiency on TMEM106B processing and the lack of specificity of the used protease inhibitors toward individual proteases, we next tested the lysosomal proteolysis of TMEM106B in HeLa KO cells for individual lysosomal soluble proteases (*CTSB*, *CTSL*, *CTSZ*, *CTSD*, *LGMN*) and multiple lysosomal proteases (*CTSB/D/L/Z/LGMN*; *CTSB/D/Z/L* and *CTSB/D/L*) (Figure 2E). Detection of endogenous TMEM106B revealed the generation of the luminal domain as two distinct bands with subtle differences in the ratio between the two distinguishable bands in individual protease-deficient cell lines and the double band of the transmembrane form, which might be explained by clonal differences between the cell lines or indirect effects of the

(E) Immunoblot analysis of wild-type and *Lgmn* KO mouse brain lysates with the TMEM106B luminal-domain-reactive antibody. CTSD immunoblot is shown for KO validation. GAPDH is shown as a loading control. A quantification of the signal intensity of the luminal domain/full-length protein ratio is depicted. Data are means ± SEM. Two-tailed unpaired Student's t tests: ns $p > 0.05$ and $^*p \leq 0.05$.

(F) Immunoblot analysis of lysates of wild-type, individual lysosomal protease KO, and multiple protease KO HeLa cells with the TMEM106B luminal-domain-reactive antibody. Immunoblots with antibodies against CTSD, CTSB, CTSZ, and CTSL are shown for protease KO confirmation. GAPDH is shown as a loading control.

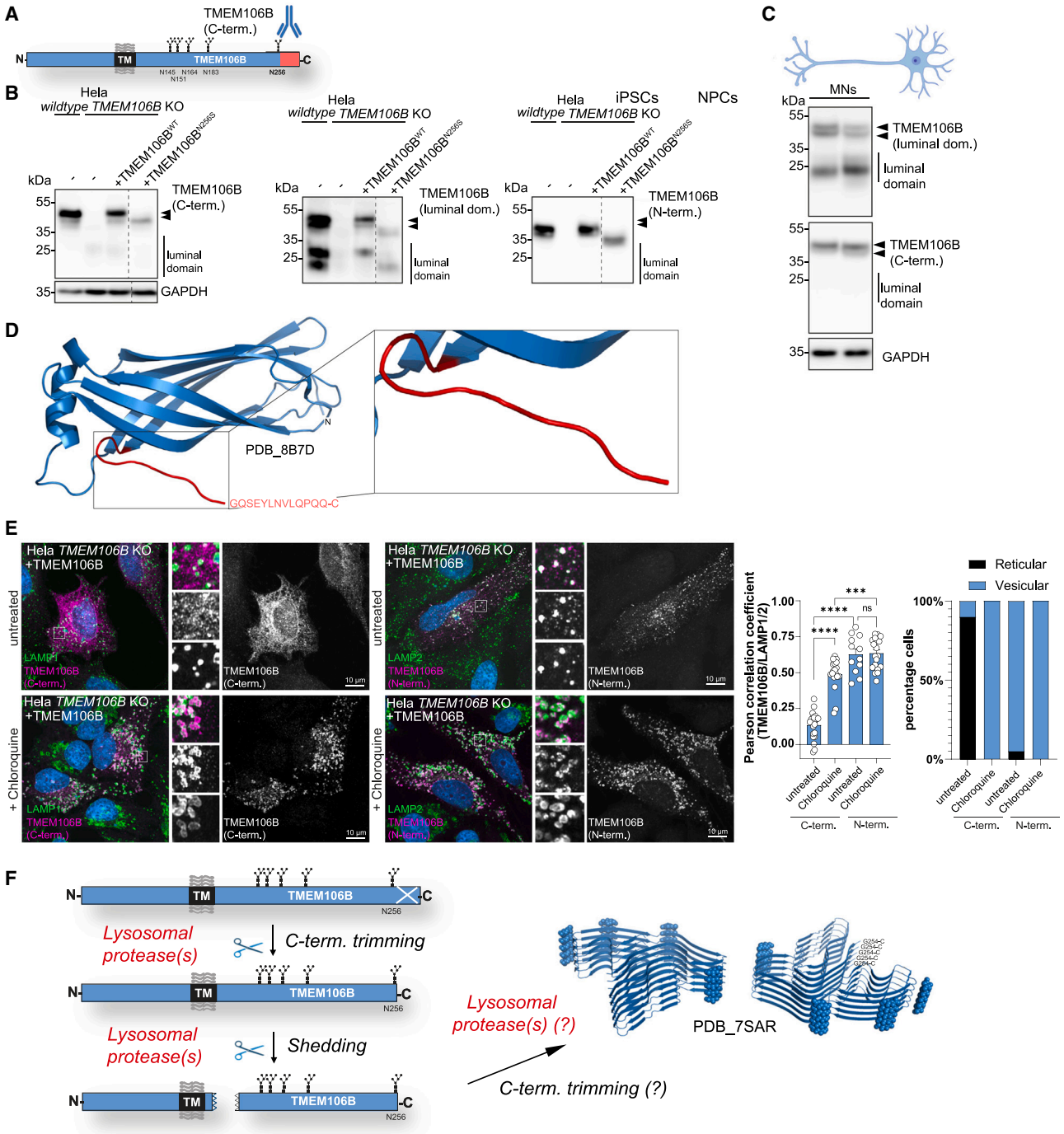


**Figure 3. Lysosomal proteases proteolytically trim the C terminus of TMEM106B**

(A) Schematic representation of the epitope for the C-terminus-specific antibody.

(B) Immunoblot analysis of lysates of wild-type HeLa cells, *TMEM106B* KO HeLa cells, *TMEM106B* KO HeLa cells re-transfected with wild-type TMEM106B, and the TMEM106B p.D256N mutant with the indicated TMEM106B-specific antibodies. GAPDH is shown as a loading control.

(C) Immunoblot analysis of two technical replicates of iPSCs differentiated to MNs with the indicated antibodies for endogenous TMEM106B. GAPDH is depicted as a loading control.

(D) Crystal structure of TMEM106B (PDB: 8B7D). The last crystallized C-terminal nine aa (p.S159–p.Leu168) are highlighted in red. The remaining 13 C-terminal aa, GQSEYLNVLQPQQ, were not resolved in the crystal structure.

(E) Immunofluorescence staining of *TMEM106B* KO HeLa cells re-transfected with untagged TMEM106B and stained treated with or without chloroquine with antibodies against the TMEM106B C terminus (magenta, left) or the N terminus (magenta, right). LAMP1/2 are depicted in green and nuclei with DAPI in blue. The

*(legend continued on next page)*

proteases on each other. In contrast, in cells deficient in the major lysosomal proteases (CTSB/D/L/Z/LGMN), the luminal domain was undetectable, revealing that the conversion of the upper band to the lower band of the full-length proteins was also inhibited. In lysates from cells deficient for four (CTSB/D/Z/L) or three (CTSB/D/L) lysosomal proteases, we only detected the upper band of the luminal domain, but both bands for the full-length protein were present. These results, in summary, suggest that different lysosomal cysteine/aspartic peptidases are physiological TMEM106B sheddases, and lysosomal proteases catalyze the conversion of the upper to the lower band of the double band of full-length TMEM106B. The analysis of brain lysates from KO mice for legumain (previously shown to be modulated by progranulin/granulins[27]) revealed a modest increase in the levels of the luminal domain of TMEM106B and, interestingly, a slight shift toward a higher-molecular-weight form (Figure 2F). CTSD, a substrate of legumain, was not processed to its double-chain form. These data rule out that legumain alone is the physiological TMEM106B sheddase.

## TMEM106B is proteolytically trimmed at the C terminus

The TMEM106B fibril cryo-EM structures cover only parts of the luminal domain from p.S120 to p.G254. While p.S120 is buried within the fibril core, p.G254 is free, and it is unclear from the cryo-EM if the remaining 20 C-terminal residues are flexible or cleaved off by proteolysis.[16–18,23] To address this question experimentally, we generated a monoclonal antibody against the very C terminus of TMEM106B (synthetic peptide antigen corresponding to residues 259–274 of human TMEM106B) (Figure 3A). The specificity of the antibody was validated in wild-type and *TMEM106B* KO HeLa cells, which we re-transfected with wild-type TMEM106B or a deletion construct lacking aa 254–275 (Figure S3A). We performed immunoblot analyses of untransfected wild-type HeLa cells, *TMEM106B* KO HeLa cells, and *TMEM106B* KO HeLa cells re-transfected with wild-type TMEM106B or a variant in which the last C-terminal N-glycosylation motif is mutated (p.N256S) with the C-terminus-specific antibody and antibodies against the luminal domain or the N terminus (Figure 3B). These experiments revealed the detection of full-length TMEM106B with the C-terminus-specific antibody as a single (upper) band and not as a double band as observed with the other two antibodies, suggesting that the ~42/44 kDa double band corresponds to the full-length protein and C-terminally trimmed full-length protein. Notably, the luminal domain was not detected with the C-terminus-specific antibody, suggesting cleavage of the C terminus before or in parallel to shedding. Another interesting finding with the p.N256S mutant was that both the full-length TMEM106B and the luminal domain shifted toward a lower molecular weight (as expected due to the lack of one N-glycan), indicating that p.N256 is still included in the physiologically generated luminal domain. This is important, given that the last resolved residue in the cryo-EM of fibrils is p.G254, suggesting either C-terminal trimming of fibrillary TMEM106B that differs from the luminal domain generated under physiological conditions or that fibrils still contain the C terminus but it was not resolved in the structures. Similar results were observed when analyzing endogenous TMEM106B in iPSC-derived human MNs, where the C-terminus-specific antibody detected only the upper band of the 42/44 kDa doublet and not the shedded luminal domain (Figure 3C). Notably, the crystal structure of native TMEM106B covered the C terminus only until residue 261,[13] likely because the remaining residues are too flexible, and it revealed the last ~20 aa as a loosely unstructured appendage without secondary structure (Figure 3D).

To get insight into where C-terminal cleavage occurs, we re-expressed TMEM106B in *TMEM106B* KO HeLa cells and performed immunofluorescence staining with and without chloroquine or BafA1 treatment (Figures 3E and S3B), which inhibits the proteolytic conversion of the upper band of the full-length double band to the lower (Figure 2A). While TMEM106B was detected in an endoplasmic-reticulum-like pattern in untreated cells, TMEM106B co-localized largely with LAMP1/2 upon inhibitor treatment, suggesting that C-terminal trimming occurs rapidly in lysosomes in untreated cells and that untrimmed full-length 44 kDa TMEM106B is only stable upon the inhibition of lysosomal proteases (Figures 3E and S3B). Our data suggest an ordered sequence of proteolysis events with C-terminal trimming followed by shedding. In lysosomes, the majority of TMEM106B is found as a C-terminally trimmed luminal domain released by shedding (Figure 3F).

## The protective TMEM106B variant does not affect shedding, and progranulin deficiency leads to altered processing of the luminal domain in mouse models

SNPs in *TMEM106B* are important disease modulators, and one coding SNP (p.T185S in humans /p.T186S in mice) is protective in human *GRN* carriers. How the SNP confers its disease-modulating function is unknown. We therefore tested if the p.T186S variant altered the proteolytic formation of the luminal domain (which might be a prerequisite for the formation of TMEM106B fibrils) by analyzing *Tmem106b* T186S knockin mice[28] and evaluated the proteolytic processing of TMEM106B in *Grn* KO mice (Figure 4A). In agreement with our previous data, we did not observe any differences in the levels of full-length TMEM106B in *Tmem106b*$^{S186/S186}$ mice compared to the wild type, but importantly, there were no significant differences in the formation of the luminal domain, suggesting that shedding is unaffected by the aa exchange. In an independent approach, we re-transfected the p.T186 variant or the p.S186 variant in *TMEM106B* KO HeLa cells and performed immunoblot analysis. Similar to the mouse brain, no major differences in the formation of the luminal domain could be observed (Figure 4B). Next, we analyzed brain lysates from *Grn* KO mice by immunoblot (Figure 4C). Full-length TMEM106B levels were upregulated (as described before[29]), but the luminal domain of TMEM106B increased to a similar extent to the full-length protein, suggesting no major effect of a progranulin deficiency on the formation

Pearson correlation coefficient between TMEM106B and LAMP1/2 is shown. One-way ANOVA. Data are means ± SEM; ***$p \leq 0.001$ and ****$p \leq 0.0001$. A quantification of the number of cells with a reticular/vesicular staining pattern is depicted.

(F) Schematic representation of the proteolytic processing of TMEM106B according to our experimental results. It is unclear whether additional C-terminal trimming occurs C-terminal to p.N256 before forming fibrils (fibril structure: PDB: 7SAR; N-glycans depicted as balls).

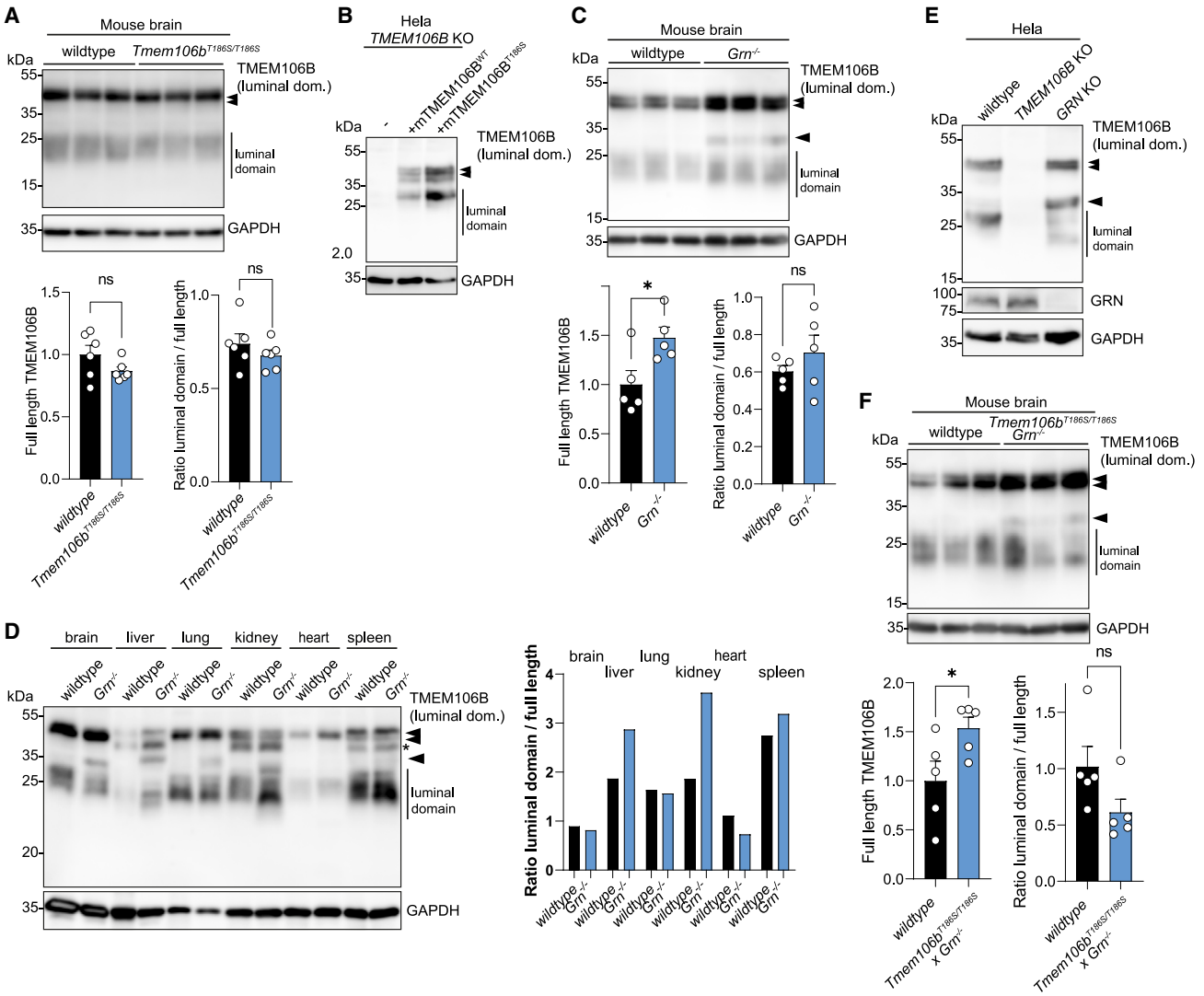


**Figure 4. The protective SNP in TMEM106B has no effect on the shedding of TMEM106B, and *Grn* KO mice show alterations in the processing of the luminal domain of TMEM106B**

(A) Immunoblot analysis of brain lysates of wild-type and *Tmem106b*$^{T186S/T186S}$ knockin mice (age: 6 months) with the TMEM106B luminal-domain-reactive antibody. GAPDH is shown as a loading control. A quantification of the signal intensity of the ratio of the luminal domain/full-length protein is depicted. Data are means ± SEM. Two-tailed unpaired Student's t tests: ns $p > 0.05$.

(B) Immunoblot analysis of *TMEM106B* KO HeLa cell lysate transfected with plasmids coding for wild-type mouse TMEM106B (mTMEM106B$^{WT}$) or the p.S186 variant (mTMEM106B$^{T186S}$) with an antibody against the luminal domain of TMEM106B. GAPDH is shown as a loading control.

(C) Immunoblot analysis of brain lysates of wild-type and *Grn* KO mice (age: 6 months) with the TMEM106B luminal-domain-reactive antibody. GAPDH is shown as a loading control. A quantification of the signal intensity of the luminal domain/full-length protein is depicted. Data are means ± SEM. Two-tailed unpaired Student's t tests: ns $p > 0.05$ and *$p \leq 0.05$.

(D) Immunoblot analysis of tissue lysates of wild-type and *Grn* KO mice with the TMEM106B luminal-domain-reactive antibody. GAPDH is shown as a loading control.

(E) Immunoblot analysis of wild-type, *TMEM106B* KO, and *GRN* KO HeLa cells with an antibody against the luminal domain of TMEM106B. GAPDH is shown as a loading control.

(F) Immunoblot analysis of brain lysates of wild-type and *Tmem106b*$^{T186S/T186S}$ x *Grn* KO mice (age: 6 months) with the TMEM106B luminal-domain-reactive antibody. GAPDH is shown as a loading control. A quantification of the signal intensity of the luminal domain/full-length protein ratio is depicted. Data are means ± SEM. Two-tailed unpaired Student's t tests: ns $p > 0.05$ and *$p \leq 0.05$.

of the luminal domain. Notably, an additional band with an apparent molecular weight of ~28–30 kDa appeared above the diffuse ~25 kDa band(s) typically observed in wild-type brain lysates (Figure 4C). This additional band was present in brain lysates from mice at 4 months (pre-symptomatic) and 12 months of age to the same extent and was also detectable in tissues other than the brain (lung, kidney) (Figures 4D and S4). Furthermore, the migration pattern of the luminal domain shifted slightly

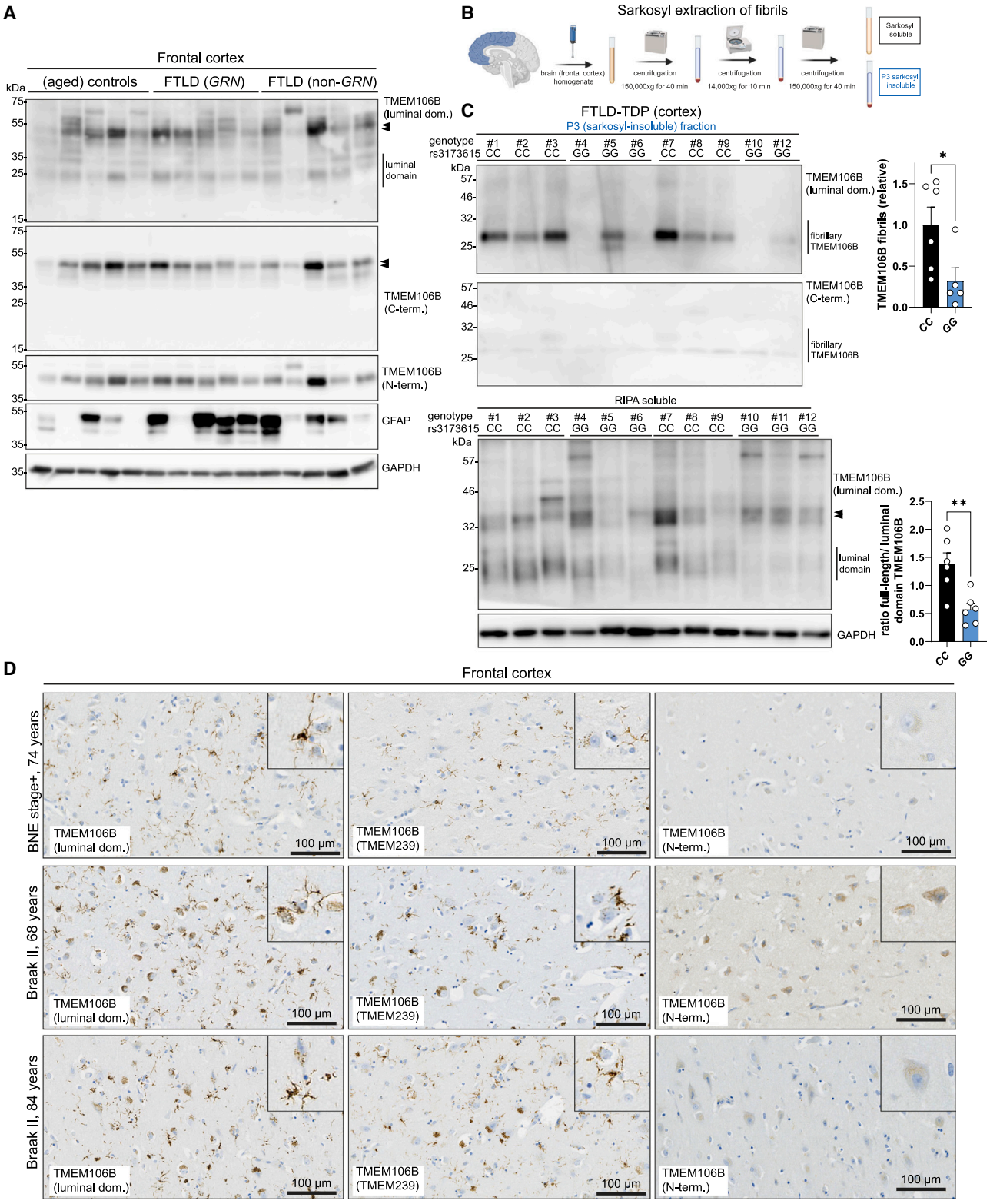


*(legend on next page)*

toward a lower molecular weight in the lysates of the brain and other tissues. *GRN* HeLa KO cells also showed an additional band for the luminal domain, suggesting a more direct effect of progranulin on TMEM106B proteolysis (Figure 4E), suggesting a direct or, more likely, an indirect effect of progranulin or granulins on the processing of TMEM106B and establishing a biochemical link. Finally, we analyzed brain lysates from *Grn* KO mice in the *Tmem106b*$^{S186/S186}$ background to test if the effects on proteolysis are due to the aa (p.T186S) exchange in TMEM106B (Figure 4F). However, the migration pattern of the luminal domain was very similar to that of *Grn* KO mice in the wild-type *Tmem106b* background, underscoring that the additional band is a consistent finding but independent of the T186S variant.

### The luminal domain-reactive antibody detects fibrillary TMEM106B in the human brain

We then tested the #SY-118C4 commercially available antibody to see if it also detected the TMEM106B luminal domain in primary human brain material. First, total brain lysates from healthy controls, patients with FTLD carrying heterozygous *GRN* mutations (FTLD-*GRN*), and patients with FTLD without diagnosed *GRN* mutations were analyzed by immunoblot (Figure 5A). GFAP immunoblotting revealed varying but obvious gliosis in most cases. Case details are provided in Table S1. Like the mouse brain, full-length TMEM106B was detected at ~44 kDa, and the luminal domain was detected as a smear at ~25 kDa, confirming that a significant amount of TMEM106B undergoes proteolysis. No major differences were observed between healthy elderly individuals and FTLD cases (both *GRN* diagnosed and non-*GRN* diagnosed). A sharp band at 44 kDa was detected only with the C-terminal antibody, not the luminal domain, which agrees with our cell-based experiments. Next, we tested whether the antibody recognized fibrillary TMEM106B by immunoblot (Figures 5B and 5C). Fibrillary TMEM106B was isolated by sarkosyl extraction (Figure 5B) and separated by SDS-PAGE, followed by immunoblot detection with the luminal domain-reactive- and the C-terminus-specific antibodies (Figure 5C). A sharp ~25 kDa band was detected, in contrast to the diffuse bands of the luminal domain in total lysates or radioimmunoprecipitation assay (RIPA) buffer lysates. It has previously been shown that individuals harboring the protective *TMEM106B* SNP (rs3173615) (C>G; p.T185S; C = risk allele, G = protective allele) have a lower TMEM106B fibril burden,[23,30] and we tested the antibody in validated cases.[23] Case details are provided in Table S2. Robust detection of fibrils was observed in 6 cases with the "CC" genotype, whereas fibrillar TMEM106B was only robustly detected in one case with the "GG" genotype. Notably, no fibrillary sarkosyl-insoluble TMEM106B was detectable with the C-terminal antibody, substantiating the interpretation that the C terminus is cleaved before fibril formation. In RIPA-soluble lysates from the same cases, we detected both full-length TMEM106B and the luminal domain, but even in our small cohort ($n$ = 6 CC/GG), we already observed significantly less shedding in GG cases, suggesting a correlation between shedding aa and fibrillary TMEM106B. These data are in agreement with previous mass-spectrometry-based experimental data.[23] Notably, in contrast to the sarkosyl-insoluble fractions, the physiological luminal domain was detected as a diffuse band, similar to the mouse brain.

Finally, we tested the #SY-118C4 monoclonal antibody for its ability to detect TMEM106B by immunohistochemistry on human brain sections of elderly individuals, given the importance of diagnostics. The antibody against the luminal domain robustly detected TMEM106B in these aged cases in a comparable pattern in glia cells and neurons to the TMEM106B antibody TMEM239 described before[18] (Figure 5D). In neurons, granular staining (typical for lysosomes) was observed, indicating that, most likely, both fibrillary and physiological TMEM106B are detected. Full-length TMEM106B (detected with an N-terminus-specific antibody) was only detected in the granular lysosomal staining pattern.

## DISCUSSION

Our data provide experimental evidence that TMEM106B undergoes two proteolytic processing events: the release of the luminal domain from its transmembrane form and the cleavage of a C-terminal peptide of the last <18 C-terminal aa. Notably, both events occur under physiological conditions. While the cleavage of the C terminus seems complete, the luminal domain's release might follow a slower kinetic. The conversion of the type II transmembrane protein to a soluble domain is strongly reminiscent of PLD3, another lysosomal type II transmembrane protein that is converted to a soluble domain within lysosomes.[31]

In our inhibitor experiments, small molecules affecting lysosomal acidification (BafA1, $NH_4Cl$, chloroquine) entirely prevented the release of the luminal domain, indicating that this cleavage occurs in acidic compartments/lysosomes. The exact cleavage site for the release (shedding) remains to be determined, but the sarkosyl-insoluble fibrils start with p.S120,[16–18] suggesting that the cleavage might occur between aa R119 and S120. A hydrophobic surface patch at the end of the luminal domain lacking a flexible linker sequence suggests it might be

**Figure 5. Formation of the luminal domain in the human brain and detection of fibrillary TMEM106B in sarkosyl-insoluble fractions with the luminal-domain-reactive antibody**

(A) Immunoblot analysis of human brain (frontal cortex) lysates of five control cases, five FTLD-*GRN* cases, and five cases without FTLD*GRN* diagnosis with TMEM106B luminal-domain-reactive antibody and the C-/N-terminus-specific antibodies and an antibody against GFAP. GAPDH is shown as a loading control.

(B) Scheme of the sarkosyl-extraction protocol for TMEM106B fibrils from the human brain.

(C) Immunoblot analysis of Sarkosyl-insoluble fractions with the TMEM106B luminal-domain-specific antibody and the C-terminus-specific antibody (top). RIPA soluble lysates were probed with the antibody against the luminal domain of TMEM106B. Note: in one case, no sarkosyl-insoluble material was available (#11). A quantification of the signal intensity for the luminal-domain-specific antibody is given. Data are means ± SEM. Two-tailed unpaired Student's t tests: $^*p \leq 0.05$.

(D) Immunohistochemical staining of the frontal cortex of human subjects with antibodies against the luminal domain of TMEM106B (Synaptic Systems, luminal domain; left), TMEM239 (middle), and the N terminus (right). BBNE, BrainNet Europe.

positioned close to the membrane.[18] In this regard, TMEM106B differs from PLD3, which has a long, flexible linker.[32] Moreover, it was speculated that this hydrophobic patch in TMEM106B might not be accessible by lysosomal proteases and that shedding occurs non-canonically.[18] Therefore, we tested if the intramembrane protease SPPL2A might be responsible for TMEM106B shedding. SPPL2A mainly cleaves as an intramembrane protease within transmembrane segments of type II proteins[25,33] and was shown before to cleave an N-terminal fragment of TMEM106B.[15] More recently, it was also shown that SPPL2A can act as a non-canonical sheddase for TNF-$\alpha$,[24] making it a prime candidate for TMEM106B shedding. However, shedding was unimpaired in brain lysates of *Sppl2a* KO mice and $(Z\text{-}LL)_2$ ketone-treated cells, ruling out that SPPL2A is a critical or essential physiological TMEM106B sheddase. The additional KO of *Sppl2b* (*Sppl2a*/*Sppl2b* double-KO mice) had only a very limited effect with a subtle decrease of the luminal domain, which is likely secondary. Moreover, we did not detect any accumulating N-terminal fragments with an antibody against the N terminus of TMEM106B on the endogenous level, making the contribution of SPPL2A (and possibly SPPL2B) to the processing of TMEM106B, at least under physiological conditions, questionable. The absence of the TMEM106B N-terminal fragment may be explained by the fact that the performed analysis shows "steady-state" N-terminal fragment levels, which depend on both the production and the degradation rates. Dynamic experiments, e.g., pulse-chase experiments, would be needed to fully exclude SPPL2s as TMEM106B-processing enzymes. Our data also highlight that the N terminus is likely rapidly degraded, e.g., by an endosomal sorting complexes required for transport (ESCRT)-dependent mechanism. It should also be noted that N-terminal proteolysis was previously mainly analyzed upon the overexpression of TMEM106B, a condition that causes drastically enlarged, aberrant endo-/lysosomal compartments representing highly artificial, non-physiological conditions.[15]

Our experiments in cathepsin-deficient cells revealed an almost complete abrogation of shedding in cells deficient in CTSB, CTSD, CTSL, CTSZ, and LGMN and strongly reduced in cells lacking only four lysosomal proteases. Although we cannot entirely rule out an indirect effect of the cathepsins on another yet-unidentified protease, our data suggest that soluble lysosomal cysteine-type proteases are physiological sheddases of TMEM106B and can functionally compensate for each other. The data also suggest they can access and cleave next to the hydrophobic patch.

Our data highlight the critical acidic pH of lysosomes for shedding. Lysosomal pH was shown to be elevated in other neurodegenerative diseases, including Alzheimer's disease[34] or progranulin deficiency in a mouse model.[35] Moreover, general lysosomal dysfunction has been observed in various neurodegenerative diseases and might negatively affect the shedding of TMEM106B. Future studies should address how far the shedding/proteolysis of TMEM106B is affected under such conditions and if possibly impaired TMEM106B shedding contributes to disease.

A very interesting finding from our study was experimental evidence of the proteolysis of a C-terminal peptide of TMEM106B. Like shedding, C-terminal trimming could be entirely prevented by pharmacologically inhibiting lysosomal acidification and the protease inhibitor leupeptin, and it was absent in cells deficient for the major lysosomal cathepsins. So far, whether this proteolytic cleavage occurs at all or under physiological conditions has been unclear. We detected the transmembrane-domain-containing TMEM106B regularly as a double band, as described before,[12] suggesting that these correspond to the full-length transmembrane proteins with and without the very C-terminal aa stretch. Moreover, it was shown before that this doublet is not due to differential N-glycosylation.[12] From the cryo-EM studies of TMEM106B fibrils, it became evident that the last aa of the fibril core was p.G254. Notably, p.G254 is solvent exposed (Figure 3E). While two studies speculated that the C-terminal 20 residues (including the N-glycosylated N256) outside the core are probably disordered,[17,18] another study suggested these last aa to be additionally removed by proteolysis.[16] Our data experimentally confirm this assumption, as the C-terminus-specific antibody could not detect sarkosyl-insoluble TMEM106B fibrils.

The last ~20 C-terminal aa of TMEM106B are not part of the native globular folded immunoglobulin-like domain and could not be crystalized/could only be crystallized up to aa L261 in a structure determination approach of the luminal domain, suggesting high flexibility.[13] This flexibility presumably makes the C terminus highly susceptible to cleavage by lysosomal cathepsin proteases. However, one crucial finding with our antibody against this very C-terminal peptide revealed that it does not detect the released luminal domain, suggesting that the C-terminal trimming precedes shedding. This finding is in good agreement with detecting the double band corresponding to full-length TMEM106B and the C-terminally trimmed transmembrane form. Another important finding was that at least p.N256 is still part of the native luminal domain, as a p.N256A mutant revealed a clear shift of the luminal domain toward a lower molecular weight due to the lack of one N-glycan. It could not be ruled out that the p.N256A mutation, however, might alter the cleavage. These results suggest that further C-terminal trimming of the luminal domain occurs before fibril formation or that the fibrils might still contain additional disordered C-terminal aa, as speculated by Jiang et al.[17] and Schweighauser et al.[18] The exact cleavage site at the C terminus, however, remains to be determined. While our data indicate that fibrils do not contain the very C terminus, it remains open to what extent C-terminal trimming affects the fibril formation or if it is a prerequisite. The physiological luminal domain was usually detected (both in the mouse brain and human brain/cell lines) as a diffuse mixture of bands of slightly different molecular weights, while the fibrils were detected as one sharp band, pointing toward additional modifications before fibril formation, e.g., proteolysis or modifications of the N-glycans.

So far, it is unknown whether variants in the aa sequence of TMEM106B modulate the risk for forming fibrils or environmental factors (activity changes of proteases, pH, etc.). One attractive hypothesis is that the physiological formation of the luminal domain is a prerequisite, and higher levels of the luminal domain also lead to higher amounts of fibrils. Recently, a clear correlation was found between the *TMEM106B* genotype for the protective SNP (p.S185) and the amounts of fibrils.[23,30] While p.T185 carriers (corresponding to the CC genotype) had

extensive levels of fibrillary TMEM106B, p.S185 (GG genotype) carriers were almost entirely devoid of TMEM106B fibrils, strongly suggesting the effects of the T/S variant on the formation of fibrils (Figure 5C). Here, we could directly correlate the amounts of the native luminal domain with fibrillary TMEM106B, and our data support the idea that p.T185 is more prone to shedding. Our data from *Tmem106b*$^{S186/S186}$ knockin mice suggest no major effect of the aa variant on the generation of the fibrils, and additional work is needed to fully elucidate the effect on shedding.

Interestingly, we observed an additional TMEM106B-related band (presumably the luminal domain) in the brain lysates of *Grn* KO mice. To the best of our knowledge, this is the first report showing an effect of progranulin deficiency on TMEM106B proteolysis. However, whether this additional polypeptide is relevant for the formation of fibrils or pathology in *GRN* carriers remains to be determined. In primary brain material from FTLD-*GRN* carriers, we did not see any evidence for this additional band. However, those patients are heterozygous for loss-of-function *GRN* mutations and still have one intact allele. How progranulin deficiency affects TMEM106B proteolysis will be subject to further investigation.

### Limitations of the study

Our data provide compelling evidence that proteolytic processing of TMEM106B is a physiological process. A question that remains to be addressed is which physiological function the luminal domain has and, moreover, how the non-physiological/pathological fibrils affect lysosomal function. More work is needed, e.g., by targeting the luminal domain to lysosomes to further understand how it affects lysosomal function, e.g., by inducing lysosomal membrane permeabilization or other critical lysosomal functions.

A technical limitation of our study is the lack of spatial data, i.e., the localization of the luminal domain under different conditions by microscopy. The luminal-domain-reactive antibody only works for immunocytochemistry upon strong, artificial overexpression, and additional antibodies are needed to address localization-related questions.

Our genetic experiments suggest that SPPL2s do not play a critical role in the shedding of TMEM106B or the degradation of the N-terminal fragment, but a contribution cannot yet be formally ruled out.

All available antibodies so far likely detect both the physiological luminal domain and fibrillary (luminal domain) of TMEM106B, making a distinction by histology impossible. Fibril-specific antibodies will be critical tools to detect exclusively pathological fibrillar TMEM106B.

## RESOURCE AVAILABILITY

### Lead contact

Further information and requests for resources and reagents should be directed to and will be fulfilled by the lead contact, Markus Damme (mdamme@biochem.uni-kiel.de).

### Materials availability

Primary materials generated during this study are available upon request through the lead contact.

### Data and code availability

- All data reported in this paper will be shared by the lead contact upon request.
- This paper does not report original code.
- Any additional information required to reanalyze the data reported in this work is available from the lead contact upon request.

## ACKNOWLEDGMENTS

Parts of some figures were created with BioRender.com. King's College London Neurodegenerative Diseases Brain Bank (funded by MRC and BDR) is acknowledged for providing human brain material. The authors wish to thank Eija Rahunen and Minna Turunen for technical support with immunohistochemistry. Manuel Schweighauser is acknowledged for the gift of the TMEM239 antibody. The research project was supported by grants from the Alzheimer's Association through the AD Strategic Fund (ADSF-21-831212-C and ADSF-24-1284323 to M.D. and ADSF-24-1284326-C to M.H. and T.R.). The research project has received the support of ELA International (agreement reference no. 2023-008I3 [M.D.]). M.P. is supported by R01NS120992 and U54NS123743. M.H. received funding from Research Council of Finland grant 338182, the Sigrid Jusélius Foundation, and The Strategic Neuroscience Funding of the University of Eastern Finland. Microscopy was supported by the DFG (INST257/640-1FUGG).

## AUTHOR CONTRIBUTIONS

S.H., S.K., F.B., N.J.G., S.-P.J., A.C., and T.M. performed the experimental work. C.E., R.F., C.K., and A.C. provided critical reagents (monoclonal antibodies) published in this study. B.S., D.W.D., T.R., L.P., and M.P. provided critical samples. L.P., M.P., M.H., P.L., A.C., and M.D. supervised experimental work and contributed to the study design. M.D. designed the experiments and wrote the manuscript. All authors approved the final manuscript.

## DECLARATION OF INTERESTS

C.E. is an employee at Synaptic Systems GmbH.

## STAR★METHODS

Detailed methods are provided in the online version of this paper and include the following:

- KEY RESOURCES TABLE
- EXPERIMENTAL MODEL AND STUDY PARTICIPANT DETAILS
  - Mouse strains and animal husbandry
  - Human postmortem samples
  - Human induced pluripotent stem cells (hiPSCs)
- METHOD DETAILS
  - Antibodies and reagents
- QUANTIFICATION AND STATISTICAL ANALYSIS

## SUPPLEMENTAL INFORMATION

Supplemental information can be found online at https://doi.org/10.1016/j.celrep.2024.115107.

Received: June 17, 2024
Revised: October 8, 2024
Accepted: December 3, 2024

## REFERENCES

1. Todd, T.W., Shao, W., Zhang, Y.J., and Petrucelli, L. (2023). The endolysosomal pathway and ALS/FTD. Trends Neurosci. *46*, 1025–1041. https://doi.org/10.1016/j.tins.2023.09.004.

2. Neefjes, J., and van der Kant, R. (2014). Stuck in traffic: an emerging theme in diseases of the nervous system. Trends Neurosci. *37*, 66–76. https://doi.org/10.1016/j.tins.2013.11.006.

3. van der Zee, J., Van Langenhove, T., Kleinberger, G., Sleegers, K., Engelborghs, S., Vandenberghe, R., Santens, P., Van den Broeck, M., Joris, G., Brys, J., et al. (2011). TMEM106B is associated with frontotemporal lobar degeneration in a clinically diagnosed patient cohort. Brain *134*, 808–815. https://doi.org/10.1093/brain/awr007.

4. Finch, N., Carrasquillo, M.M., Baker, M., Rutherford, N.J., Coppola, G., Dejesus-Hernandez, M., Crook, R., Hunter, T., Ghidoni, R., Benussi, L., et al. (2011). TMEM106B regulates progranulin levels and the penetrance of FTLD in GRN mutation carriers. Neurology *76*, 467–474. https://doi.org/10.1212/WNL.0b013e31820a0e3b.

5. Cruchaga, C., Graff, C., Chiang, H.H., Wang, J., Hinrichs, A.L., Spiegel, N., Bertelsen, S., Mayo, K., Norton, J.B., Morris, J.C., and Goate, A. (2011). Association of TMEM106B gene polymorphism with age at onset in granulin mutation carriers and plasma granulin protein levels. Arch. Neurol. *68*, 581–586. https://doi.org/10.1001/archneurol.2010.350.

6. Van Deerlin, V.M., Sleiman, P.M.A., Martinez-Lage, M., Chen-Plotkin, A., Wang, L.S., Graff-Radford, N.R., Dickson, D.W., Rademakers, R., Boeve, B.F., Grossman, M., et al. (2010). Common variants at 7p21 are associated with frontotemporal lobar degeneration with TDP-43 inclusions. Nat. Genet. *42*, 234–239. https://doi.org/10.1038/ng.536.

7. Cherry, J.D., Mez, J., Crary, J.F., Tripodis, Y., Alvarez, V.E., Mahar, I., Huber, B.R., Alosco, M.L., Nicks, R., Abdolmohammadi, B., et al. (2018). Variation in TMEM106B in chronic traumatic encephalopathy. Acta Neuropathol. Commun. *6*, 115. https://doi.org/10.1186/s40478-018-0619-9.

8. Nelson, P.T., Wang, W.X., Partch, A.B., Monsell, S.E., Valladares, O., Ellingson, S.R., Wilfred, B.R., Naj, A.C., Wang, L.S., Kukull, W.A., and Fardo, D.W. (2015). Reassessment of risk genotypes (GRN, TMEM106B, and ABCC9 variants) associated with hippocampal sclerosis of aging pathology. J. Neuropathol. Exp. Neurol. *74*, 75–84. https://doi.org/10.1097/NEN.0000000000000151.

9. Dugan, A.J., Nelson, P.T., Katsumata, Y., Shade, L.M.P., Boehme, K.L., Teylan, M.A., Cykowski, M.D., Mukherjee, S., Kauwe, J.S.K., Hohman, T.J., et al. (2021). Analysis of genes (TMEM106B, GRN, ABCC9, KCNMB2, and APOE) implicated in risk for LATE-NC and hippocampal sclerosis provides pathogenetic insights: a retrospective genetic association study. Acta Neuropathol. Commun. *9*, 152. https://doi.org/10.1186/s40478-021-01250-2.

10. Bellenguez, C., Küçükali, F., Jansen, I.E., Kleineidam, L., Moreno-Grau, S., Amin, N., Naj, A.C., Campos-Martin, R., Grenier-Boley, B., Andrade, V., et al. (2022). New insights into the genetic etiology of Alzheimer's disease and related dementias. Nat. Genet. *54*, 412–436. https://doi.org/10.1038/s41588-022-01024-z.

11. Simons, C., Dyment, D., Bent, S.J., Crawford, J., D'Hooghe, M., Kohlschütter, A., Venkateswaran, S., Helman, G., Poll-The, B.T., Makowski, C.C., et al. (2017). A recurrent de novo mutation in TMEM106B causes hypomyelinating leukodystrophy. Brain *140*, 3105–3111. https://doi.org/10.1093/brain/awx314.

12. Lang, C.M., Fellerer, K., Schwenk, B.M., Kuhn, P.H., Kremmer, E., Edbauer, D., Capell, A., and Haass, C. (2012). Membrane orientation and subcellular localization of transmembrane protein 106B (TMEM106B), a major risk factor for frontotemporal lobar degeneration. J. Biol. Chem. *287*, 19355–19365. https://doi.org/10.1074/jbc.M112.365098.

13. Baggen, J., Jacquemyn, M., Persoons, L., Vanstreels, E., Pye, V.E., Wrobel, A.G., Calvaresi, V., Martin, S.R., Roustan, C., Cronin, N.B., et al. (2023). TMEM106B is a receptor mediating ACE2-independent SARS-CoV-2 cell entry. Cell *186*, 3427–3442.e22. https://doi.org/10.1016/j.cell.2023.06.005.

14. Levine, T.P. (2022). TMEM106B in humans and Vac7 and Tag1 in yeast are predicted to be lipid transfer proteins. Proteins *90*, 164–175. https://doi.org/10.1002/prot.26201.

15. Brady, O.A., Zhou, X., and Hu, F. (2014). Regulated intramembrane proteolysis of the frontotemporal lobar degeneration risk factor, TMEM106B, by signal peptide peptidase-like 2a (SPPL2a). J. Biol. Chem. *289*, 19670–19680. https://doi.org/10.1074/jbc.M113.515700.

16. Chang, A., Xiang, X., Wang, J., Lee, C., Arakhamia, T., Simjanoska, M., Wang, C., Carlomagno, Y., Zhang, G., Dhingra, S., et al. (2022). Homotypic fibrillization of TMEM106B across diverse neurodegenerative diseases. Cell *185*, 1346–1355.e15. https://doi.org/10.1016/j.cell.2022.02.026.

17. Jiang, Y.X., Cao, Q., Sawaya, M.R., Abskharon, R., Ge, P., DeTure, M., Dickson, D.W., Fu, J.Y., Ogorzalek Loo, R.R., Loo, J.A., and Eisenberg, D.S. (2022). Amyloid fibrils in FTLD-TDP are composed of TMEM106B and not TDP-43. Nature *605*, 304–309. https://doi.org/10.1038/s41586-022-04670-9.

18. Schweighauser, M., Arseni, D., Bacioglu, M., Huang, M., Lövestam, S., Shi, Y., Yang, Y., Zhang, W., Kotecha, A., Garringer, H.J., et al. (2022). Age-dependent formation of TMEM106B amyloid filaments in human brains. Nature *605*, 310–314. https://doi.org/10.1038/s41586-022-04650-z.

19. Baggen, J., Persoons, L., Vanstreels, E., Jansen, S., Van Looveren, D., Boeckx, B., Geudens, V., De Man, J., Jochmans, D., Wauters, J., et al. (2021). Genome-wide CRISPR screening identifies TMEM106B as a proviral host factor for SARS-CoV-2. Nat. Genet. *53*, 435–444. https://doi.org/10.1038/s41588-021-00805-2.

20. Wang, R., Simoneau, C.R., Kulsuptrakul, J., Bouhaddou, M., Travisano, K.A., Hayashi, J.M., Carlson-Stevermer, J., Zengel, J.R., Richards, C.M., Fozouni, P., et al. (2021). Genetic Screens Identify Host Factors for SARS-CoV-2 and Common Cold Coronaviruses. Cell *184*, 106–119.e14. https://doi.org/10.1016/j.cell.2020.12.004.

21. Schneider, W.M., Luna, J.M., Hoffmann, H.H., Sánchez-Rivera, F.J., Leal, A.A., Ashbrook, A.W., Le Pen, J., Ricardo-Lax, I., Michailidis, E., Peace, A., et al. (2021). Genome-Scale Identification of SARS-CoV-2 and Pan-coronavirus Host Factor Networks. Cell *184*, 120–132.e14. https://doi.org/10.1016/j.cell.2020.12.006.

22. Stagi, M., Klein, Z.A., Gould, T.J., Bewersdorf, J., and Strittmatter, S.M. (2014). Lysosome size, motility and stress response regulated by fronto-temporal dementia modifier TMEM106B. Mol. Cell. Neurosci. *61*, 226–240. https://doi.org/10.1016/j.mcn.2014.07.006.

23. Marks, J.D., Ayuso, V.E., Carlomagno, Y., Yue, M., Todd, T.W., Hao, Y., Li, Z., McEachin, Z.T., Shantaraman, A., Duong, D.M., et al. (2024). TMEM106B core deposition associates with TDP-43 pathology and is increased in risk SNP carriers for frontotemporal dementia. Sci. Transl. Med. *16*, eadf9735. https://doi.org/10.1126/scitranslmed.adf9735.

24. Spitz, C., Schlosser, C., Guschtschin-Schmidt, N., Stelzer, W., Menig, S., Götz, A., Haug-Kröper, M., Scharnagl, C., Langosch, D., Muhle-Goll, C., and Fluhrer, R. (2020). Non-canonical Shedding of TNFalpha by SPPL2a Is Determined by the Conformational Flexibility of Its Transmembrane Helix. iScience *23*, 101775. https://doi.org/10.1016/j.isci.2020.101775.

25. Schneppenheim, J., Dressel, R., Hüttl, S., Lüllmann-Rauch, R., Engelke, M., Dittmann, K., Wienands, J., Eskelinen, E.L., Hermans-Borgmeyer, I., Fluhrer, R., et al. (2013). The intramembrane protease SPPL2a promotes B cell development and controls endosomal traffic by cleavage of the invariant chain. J. Exp. Med. *210*, 41–58. https://doi.org/10.1084/jem.20121069.

26. Schneppenheim, J., Hüttl, S., Mentrup, T., Lüllmann-Rauch, R., Rothaug, M., Engelke, M., Dittmann, K., Dressel, R., Araki, M., Araki, K., et al. (2014). The intramembrane proteases signal Peptide peptidase-like 2a and 2b have distinct functions in vivo. Mol. Cell Biol. *34*, 1398–1411. https://doi.org/10.1128/MCB.00038-14.

27. Robinson, S., Reich, M., Mühlhofer, M.-T., Buschmann, K., Wauters, E., Mühlhofer, Q., Werner, G., Ahles, A., Engelhardt, S., Krenner, C., et al. (2024). Enhanced legumain activity links progranulin deficiency to TDP-43 pathology in frontotemporal lobar degeneration. Preprint at bioRxiv. https://doi.org/10.1101/2024.01.16.575687.

28. Cabron, A.S., Borgmeyer, U., Richter, J., Peisker, H., Gutbrod, K., Dörmann, P., Capell, A., and Damme, M. (2023). Lack of a protective effect of the Tmem106b "protective SNP" in the Grn knockout mouse model

for frontotemporal lobar degeneration. Acta Neuropathol. Commun. *11*, 21. https://doi.org/10.1186/s40478-023-01510-3.

29. Gotzl, J.K., Mori, K., Damme, M., Fellerer, K., Tahirovic, S., Kleinberger, G., Janssens, J., van der Zee, J., Lang, C.M., Kremmer, E., et al. (2014). Common pathobiochemical hallmarks of progranulin-associated frontotemporal lobar degeneration and neuronal ceroid lipofuscinosis. Acta Neuropathol. *127*, 845–860. https://doi.org/10.1007/s00401-014-1262-6.
30. T Vicente, C., Perneel, J., Wynants, S., Heeman, B., Van den Broeck, M., Baker, M., Cheung, S., Faura, J., Mackenzie, I.R.A., and Rademakers, R. (2023). C-terminal TMEM106B fragments in human brain correlate with disease-associated TMEM106B haplotypes. Brain *146*, 4055–4064. https://doi.org/10.1093/brain/awad133.
31. Gonzalez, A.C., Schweizer, M., Jagdmann, S., Bernreuther, C., Reinheckel, T., Saftig, P., and Damme, M. (2018). Unconventional Trafficking of Mammalian Phospholipase D3 to Lysosomes. Cell Rep. *22*, 1040–1053. https://doi.org/10.1016/j.celrep.2017.12.100.
32. Roske, Y., Cappel, C., Cremer, N., Hoffmann, P., Koudelka, T., Tholey, A., Heinemann, U., Daumke, O., and Damme, M. (2024). Structural analysis of PLD3 reveals insights into the mechanism of lysosomal 5' exonuclease-mediated nucleic acid degradation. Nucleic Acids Res. *52*, 370–384. https://doi.org/10.1093/nar/gkad1114.
33. Friedmann, E., Hauben, E., Maylandt, K., Schleeger, S., Vreugde, S., Lichtenthaler, S.F., Kuhn, P.H., Stauffer, D., Rovelli, G., and Martoglio, B. (2006). SPPL2a and SPPL2b promote intramembrane proteolysis of TNFalpha in activated dendritic cells to trigger IL-12 production. Nat. Cell Biol. *8*, 843–848. https://doi.org/10.1038/ncb1440.
34. Lee, J.H., Yang, D.S., Goulbourne, C.N., Im, E., Stavrides, P., Pensalfini, A., Chan, H., Bouchet-Marquis, C., Bleiwas, C., Berg, M.J., et al. (2022). Faulty autolysosome acidification in Alzheimer's disease mouse models induces autophagic build-up of Abeta in neurons, yielding senile plaques. Nat. Neurosci. *25*, 688–701. https://doi.org/10.1038/s41593-022-01084-8.
35. Tanaka, Y., Suzuki, G., Matsuwaki, T., Hosokawa, M., Serrano, G., Beach, T.G., Yamanouchi, K., Hasegawa, M., and Nishihara, M. (2017). Progranulin regulates lysosomal function and biogenesis through acidification of lysosomes. Hum. Mol. Genet. *26*, 969–988. https://doi.org/10.1093/hmg/ddx011.
36. Luningschror, P., Werner, G., Stroobants, S., Kakuta, S., Dombert, B., Sinske, D., Wanner, R., Lullmann-Rauch, R., Wefers, B., Wurst, W., et al. (2020). The FTLD Risk Factor TMEM106B Regulates the Transport of Lysosomes at the Axon Initial Segment of Motoneurons. Cell Rep. *30*, 3506–3519.e6. https://doi.org/10.1016/j.celrep.2020.02.060.
37. Kayasuga, Y., Chiba, S., Suzuki, M., Kikusui, T., Matsuwaki, T., Yamanouchi, K., Kotaki, H., Horai, R., Iwakura, Y., and Nishihara, M. (2007). Alteration of behavioural phenotype in mice by targeted disruption of the progranulin gene. Behav. Brain Res. *185*, 110–118. https://doi.org/10.1016/j.bbr.2007.07.020.
38. Jungnickel, K.E.J., Guelle, O., Iguchi, M., Dong, W., Kotov, V., Gabriel, F., Debacker, C., Dairou, J., McCort-Tranchepain, I., Laqtom, N.N., et al. (2024). MFSD1 with its accessory subunit GLMP functions as a general dipeptide uniporter in lysosomes. Nat. Cell Biol. *26*, 1047–1061. https://doi.org/10.1038/s41556-024-01436-5.
39. Behnke, J., Schneppenheim, J., Koch-Nolte, F., Haag, F., Saftig, P., and Schröder, B. (2011). Signal-peptide-peptidase-like 2a (SPPL2a) is targeted to lysosomes/late endosomes by a tyrosine motif in its C-terminal tail. FEBS Lett. *585*, 2951–2957. https://doi.org/10.1016/j.febslet.2011.08.043.
40. Gallwitz, L., Bleibaum, F., Voss, M., Schweizer, M., Spengler, K., Winter, D., Zöphel, F., Müller, S., Lichtenthaler, S., Damme, M., and Saftig, P. (2024). Cellular depletion of major cathepsin proteases reveals their concerted activities for lysosomal proteolysis. Cell. Mol. Life Sci. *81*, 227. https://doi.org/10.1007/s00018-024-05274-4.
41. Massih, B., Veh, A., Schenke, M., Mungwa, S., Seeger, B., Selvaraj, B.T., Chandran, S., Reinhardt, P., Sterneckert, J., Hermann, A., et al. (2023). A 3D cell culture system for bioengineering human neuromuscular junctions to model ALS. Front. Cell Dev. Biol. *11*, 996952. https://doi.org/10.3389/fcell.2023.996952.

## STAR★METHODS

### KEY RESOURCES TABLE

| REAGENT or RESOURCE | SOURCE | IDENTIFIER |
|---|---|---|
| **Antibodies** | | |
| TMEM106B; luminal domain, rat monoclonal, clone #SY-118C4 | This paper | Cat#506 017, RRID: AB_3662613 |
| TMEM106B; C-terminal epitope, rat monoclonal, clone 23A12, rat IgG2b | This paper | N/A |
| TMEM239; luminal domain, rabbit polyclonal | Gift Manuel Schweighauser | N/A |
| TMEM106B; rabbit monoclonal E7H7Z | Cell Signaling | Cat#93334, RRID: AB_2924267 |
| LAMP1, rat monoclonal, clone 1D4B | DSHB | N/A |
| LAMP2, mouse monoclonal, clone H4B4 | DSHB | N/A |
| LAMP1, rabbit monoclonal, clone D2D11 | Cell Signaling | Cat#9091, RRID: AB_2687579 |
| GAPDH; mouse mAb, clone 6C5 | Santa Cruz Biotechnology | Cat#sc-32233, RRID: AB_627679 |
| Cathepsin D, rabbit polyclonal | In house | N/A |
| SPPL2A, rabbit polyclonal | Gift Bernd Schröder | N/A |
| SPPL2B, rabbit polyclonal | Gift Bernd Schröder | N/A |
| TUJ1, mouse monoclonal MO15013 | Neuromics | Cat#MO15013; RRID: AB_2737114 |
| Cathepsin B, goat polyclonal | R&D Systems | Cat#AF953, RRID: AB_355738 |
| Cathepsin L, goat polyclonal | R&D Systems | Cat#AF952, RRID: AB_355737 |
| Cathepsin Z, goat polyclonal | R&D Systems | Cat#AF934, RRID: AB_2087676 |
| Cathepsin D, goat polyclonal | R&D Systems | Cat#AF1014, RRID: AB_2087218 |
| Progranulin; rabbit polyclonal HPA008763 | Sigma Aldrich | Cat#HPA008763, RRID: AB_1850339 |
| GFAP | Sigma Aldrich | Cat# G3893, RRID: AB_477010 |
| **Biological samples** | | |
| Human postmortem brain material (cerebral cortex; fresh frozen/Paraffin-embedded) | London Brain Bank | N/A |
| Human brain material (cerebral cortex, fresh-frozen) | London Brain Bank | N/A |
| Human brain material (cerebral cortex, fresh-frozen) | Brain Bank for Neurodegenerative Disorders at Mayo Clinic Florida | N/A |
| **Chemicals, peptides, and recombinant proteins** | | |
| Recombinant Cas9 | Synthego | N/A |
| E64D | Cayman Chemical Company | N/A |
| Chloroquine | Sigma Aldrich | N/A |
| Leupeptine | Sigma Aldrich | N/A |
| Pepstatin A | Sigma Aldrich | N/A |
| $NH_4Cl$ | Sigma Aldrich | N/A |
| $(Z\text{-}LL)_2$ Ketone | Peptanova | N/A |
| Turbofect | Thermo Scientific | N/A |
| dorsomorphin homolog 1 (DMH1 | R&D Systems | N/A |
| CHIR99021 (GSK-3 inhibitor), #13122 | Cayman Chemical Company | N/A |
| Purmorphamine (PMA) | Cayman Chemical Company | N/A |
| SB431542 (TGF-β inhibitor) | AdooQ BioScience | N/A |
| ROCK Inhibitor | StemMACS™ | N/A |
| *N*-2 Supplement | Gibco | N/A |
| Ascorbic acid, #A92902 | Sigma Aldrich | N/A |
| Dibutyryl-cAMP, HY-B0764 | MedChemTronica | N/A |
| Brain-derived neurotrophic factor (BDNF), #450-02 | PeproTech | N/A |
| glia-derived neurotrophic factor (GDNF), #G-240 | Alomone Labs | N/A |

(*Continued on next page*)

| Continued | | |
|---|---|---|
| REAGENT or RESOURCE | SOURCE | IDENTIFIER |
| Retinoic acid, #72264 | Stemcell Technologies | N/A |
| **Critical commercial assays** | | |
| Vectastain Elite ABC Kit Peroxidase | Vector Laboratories | N/A |
| **Experimental models: Cell lines** | | |
| Hela | CLS Cell Lines Service | N/A |
| Human control iPSC line SCTi003-A | Stem Cell Technologies | Cat#SCTi003-A; RRID: CVCL_C1W7 |
| **Experimental models: Organisms/strains** | | |
| *Tmem106b* knockout mice | Lüningschrör et al.[36] | N/A |
| *Sppl2a* knockout mice | Schneppenheim et al.[25] | N/A |
| *Sppl2a*/*Sppl2* double knockout mice | Schneppenheim et al.[26] | N/A |
| *Lgmn* knockout mice | Robinson et al.[27] | N/A |
| *Grn* knockout mice | Kayasuga et al.[37] | N/A |
| *Tmem106b*$^{T186S}$ knockin mice | Cabron et al.[28] | N/A |
| *Tmem106b*$^{T186S}$ knockin x *Grn* knockout mice | Cabron et al.[28] | N/A |
| **Oligonucleotides** | | |
| CRISPR gRNA *TMEM106B* #1 UCUUCUUUGCUUGAAUGCAA | Synthego | N/A |
| CRISPR gRNA *TMEM106B* #2 AGUGAAGUCCAUAAUGAAGA | Synthego | N/A |
| CRISPR gRNA *TMEM106B* #3 CUUCCUGUAAAUUCCACAUA | Synthego | N/A |
| CRISPR gRNA *LGMN* GUACCAGUCCCCCAGGUACG | Synthego | N/A |
| **Recombinant DNA** | | |
| Untagged human TMEM106B in pcDNA3.1 Hygro (+) | This paper | N/A |
| **Software and algorithms** | | |
| GraphPad Prism 9.3.1 | GraphPad Software | N/A |
| ImageJ 1.46r | NIH | N/A |
| Zen 3.2 (Blue edition) | Zeiss | N/A |

## EXPERIMENTAL MODEL AND STUDY PARTICIPANT DETAILS

### Mouse strains and animal husbandry

*Tmem106b* KO mice generated by CRISPR/Cas9 mediated targeted gene disruption were described before.[36] The generation of *Sppl2a* KO mice and *Sppl2a*/*Sppl2b* double KO mice was described before[25,26]. Knockin mice containing the *Tmem106b* S186 variant (*Tmem106b*$^{T186S/T186S}$) and *Tmem106b S186* in the *Grn* KO background (*Grn* KO x *Tmem106b*$^{T186S/T186S}$) were described before.[28] *Grn* KO mice generated by targeted gene disruption were described before.[37] *Lgmn* KO mice were described before.[27]

Mice were housed under standard laboratory conditions with a 12-h light/dark cycle and constant room temperature and humidity. Food and water were available *ad libitum*. Experimental protocols were approved by the local German authorities (Ministerium für Energiewende, Landwirtschaft, Umwelt und ländliche Räume, Kiel, IX 552–65/2023 (8-2/23V; Landesdirektion Sachsen, TV vG 5/2023, 25–5131/564/5). Mice of both genders in the C57/Bl6 background were used throughout the study. Mice between 3 and 9 months were used.

### Human postmortem samples

Postmortem brain samples were obtained from the London Brain Bank and the Brain Bank for Neurodegenerative Disorders at Mayo Clinic Florida.

Details regarding the human subjects, including age and gender, can be found in the supplemental tables (Tables S1 and S2).

For sarkosyl extraction of TMEM106B fibrils (Table S2), de-identified protein samples from patients with neuropathologically confirmed frontotemporal dementia (FTD) were used in this study. Patient tissues were originally obtained from the Brain Bank for Neurodegenerative Disorders at Mayo Clinic Florida. Autopsies were performed after consent by the next-of-kin or someone with legal authority to grant permission. The Brain Bank operates under protocols approved by the Mayo Clinic Institutional Review Board (IRB).

Postmortem brain material for immunohistochemistry and total brain immunoblots was collected from donors for or from whom a written informed consent for a brain autopsy and the use of the material and clinical information for research purposes had been obtained by the MRC London Brain Bank for Neurodegenerative Diseases.

### Human induced pluripotent stem cells (hiPSCs)

iPSCs for MN differentiation were purchased from Stem Cell Technologies (SCTi003-A). The cells were originally derived from a healthy female donor. iPSCs were cultured and expanded in Essential 8 Flex Medium (Thermo Scientific #A2858501) on Matrigel-coated (1:100) (Corning, 356234) dishes. Cultures with 80%–90% confluency were split 1:5 using ReLeSR reagent (Stemcell Technologies, #05872). 10 μM ROCK Inhibitor (StemMACS Y27632) was added for 24 h after splitting.

## METHOD DETAILS

### Antibodies and reagents

#### *Chemicals and antibodies*

If not stated otherwise, analytical-grade chemicals were purchased from Sigma-Aldrich (MO, USA). Inhibitors were purchased from the following companies: E64D (Cayman Chemicals), chloroquine, leupeptin, pepstatin A, $NH_4Cl$ (Sigma-Aldrich), $(Z\text{-}LL)_2$ ketone (Peptanova).

Antibodies targeting the very C terminus of human TMEM106B were generated by immunization of Lou/c rats with an ovalbumin-coupled peptide corresponding to residues 259–274 of human TMEM106B (YQLGQSEYLNVLQPQQ; Peps4LS, Heidelberg, Germany). A boost injection was given eight weeks later, and spleen cells were fused with myeloma cell line P3 × 63-Ag8.653 (ATCC, American Type Culture Collection) by standard procedures. Hybridoma supernatants were screened in a flow cytometry assay (iQue, Intellicyt; Sartorius) for binding to biotinylated peptide coupled to streptavidin beads (PolyAN, Berlin). Positive clones were further validated in immunoblotting and subcloned by limiting dilution to obtain stable antibody-producing monoclonal cell lines.

The following primary antibodies were used for immunoblotting: TMEM106B luminal domain (rat monoclonal, clone #SY-118C4; against a synthetic peptide corresponding to residues 239–252 of human TMEM106B: C-HSEQISQERYQYVD; 1:1.000/1.4 μg/mL; cat. No. 506 017, Synaptic Systems, Göttingen, Germany). TMEM106B C-terminal (rat monoclonal, clone 23A12 against a synthetic peptide corresponding to residues 259–274 of human TMEM106B), TMEM106B (N terminus) (1:1.000, rabbit monoclonal; E7H7Z; Cell Signaling Technology), GAPDH (1:1.000, mouse monoclonal, 6C5/sc-32233; Santa Cruz Biotechnology), mouse CTSD (1:1.000, rabbit polyclonal custom-made[38]), LAMP1 (1:1.000, rat monoclonal, clone 1D4B, Developmental Studies Hybridoma Bank), LAMP2 (1:1.000 mouse monoclonal, clone H4B4, Developmental Studies Hybridoma Bank), LAMP1 (1:400, rabbit monoclonal, clone D2D11, Cell Signaling Technology), SPPL2A (1:1.000, rabbit polyclonal, described before[39]), SPPL2B (1:1.000, rabbit polyclonal, described before[26]), GRN (1:1.000, rabbit polyclonal HPA008763, Atlas Antibodies/Merck Sigma-Aldrich), CTSL (1:1.000, goat polyclonal, AF952, R&D Systems, Minneapolis, USA), CTSD (1:1.000, goat polyclonal, AF1014, R&D Systems, Minneapolis, USA), CTSZ (1:1.000, goat polyclonal, AF934, R&D Systems, Minneapolis, USA), CTSB (1:500, goat polyclonal, AF953, R&D Systems, Minneapolis, USA). Horseradish peroxidase (HRP)-coupled secondary antibodies were purchased from Dianova (Hamburg, Germany) and used in a 1:15.000 dilution.

#### *Expression constructs*

The C-terminally tagged human TMEM106B cDNA in the pcDNA3.1 Hygro(+) was described before.[12] TMEM106B was amplified by PCR and cloned with *HindIII* and *XbaI* into the pcDNA3.1 Hygro(+) expression vector for cloning an expression vector without epitope tags.

#### *Cell lines and CRISPR/Cas9-mediated gene knockout*

HeLa cell lines were cultured under standard conditions in full medium (Dulbecco's modified Eagle Medium (DMEM)) containing 4.5 g/L of D-Glucose and L-glutamine (Thermo Fisher Scientific) and were supplemented with 10% (v/v) fetal bovine serum (FBS) and 1% Penicillin/Streptomycin. Cells were cultivated in 5% $CO_2$ at 37°C *TMEM106B* CRISPR/Cas9 mediated KO cells (*TMEM106B* KO) were generated with CRISPR guide RNAs ("Gene knockout kit") from Synthego (Redwood City, CA, USA) with the following sequence: UCUUCUUUGCUUGAAUGCAA, AGUGAAGUCCAUAAUGAAGA, CUUCCUGUAAAUUCCACAUA. CRISPR/Cas9-mediated KO was performed using the Neon Transfection System (Thermo Fisher Scientific): Synthetic CRISPR guide RNAs and recombinant Cas9 (Synthego) were electroporated according to the manufacturer's protocol and recommendations. The next day, after reaching a 90% confluency, the medium was exchanged, and single-cell clones were generated by dilution-seeding in 96-well plates. The single clones were expanded for sequencing and KO validation by Sanger sequencing and the Synthego ICE Analysis Tool. The KO was additionally validated by immunoblot with specific antibodies. Individual cathepsin-deficient HeLa cells and cells deficient for four proteases (CTSB, CTSL, CTSZ, CTSD) were described previously.[40] For the generation of the cell line with an additional legumain KO of *LGMN*, the multi *CTSB/L/Z/D* KO cell line was used, and *LGMN* was additionally knocked out by CRISPR/Cas9 (guide RNA: *LGMN*: GUACCAGUCCCCCAGGUACG) (Synthego, Redwood City, CA, USA).

#### *Differentiation of motor neurons from iPSCs*

Motorneurons were differentiated as previously described with few modifications.[41] For neuronal induction, Essential 8 Flex Medium was supplemented with 10 μM SB431542 (AdooQ BioScience, #A10826-50), 1 μM dorsomorphin homolog 1 (DMH1; R&D Systems, #4126), 3 μM CHIR99021 (Cayman Chemical Company, #13122), and 0.5 μM Purmorphamine (PMA) (Cayman Chemical Company, #10009634). On day 2, the medium was changed to neuronal medium supplemented with the same small molecule supplements. Neuronal medium consisted of Neurobasal medium (Gibco, #21103049), Dulbecco's modified Eagle's medium F-12 (DMEM/F-12) (Gibco, #21331046), MACS NeuroBrew-21 (Miltenyi Biotech, #130-097-263), *N*-2 Supplement (Gibco, #17502048), 100 μg/mL Penicillin/Streptomycin/Glutamax (Gibco, #10378016). On day 4, the medium was changed to an expansion medium consisting

of neuronal medium supplemented with 3 μM CHIR99021 (Cayman Chemical Company #13122), 0.5 μM PMA and 150 μM Ascorbic acid (AA; Sigma, #A92902). 80%–90% confluent cells were split and kept in suspension on uncoated dishes. Embryoid Bodies (EBs) were formed from day 6 on in suspension and were selected and dissociated with a 1 mL pipette. Subsequently, cells were seeded on Matrigel-coated dishes. The resulting NPCs were split twice a week with Accutase (Thermo Fisher, #07920) and expanded for at least 15 passages to achieve pure NPC cultures. The medium was changed every other day.

For NPC differentiation into MNs, cells were cultured for 9 days in a neuronal medium supplemented with 1 μM PMA. From day 2 onwards, 1 μM Retinoic acid (Stemcell Technologies, #72264) was added to the medium. The medium was changed every other day. For MN differentiation, the medium was switched after 9 days to neuronal medium supplemented with 10 ng/mL glia-derived neurotrophic factor (GDNF) (Alomone Labs, #G-240), 5 ng/mL brain-derived neurotrophic factor (BDNF) (PeproTech, #450-02), and 500 μM dibutyryl-cAMP (dbcAMP; MedChemTronica, HY-B0764).

### Transfection of cultured cells

HeLa cells were purchased from CLS Cell Lines Service and used at low passage numbers. Cells were cultured in Dulbecco's modified Eagle's medium (DMEM, Gibco) supplemented with 10% (v/v) fetal bovine serum (FBS; Sigma-Aldrich) and antibiotics (penicillin-streptomycin) at 37°C in a humidified atmosphere at 5% $CO_2$. Cells were transfected with plasmid DNA using Turbofect (Thermo Scientific) based on the stable cationic polymer polyethylenimine (PEI). DNA was incubated with Turbofect in a ratio of 1 μg plasmid-DNA: 2 μL Turbofect for 20 min at room temperature. The solution was dripped onto the adherent cells in DMEM containing 10% FCS. The medium was changed 6 h after the addition of the Turbofect-plasmid complex.

### Immunocytochemistry

Immunocytochemistry was performed as previously described.[31] Briefly, semi-confluent cells were seeded and grown on coverslips and fixed with 4% (w/v) paraformaldehyde (PFA; Roth) in PBS for 20 min at room temperature. After permeabilization of the cells with 0.2% (w/v) saponin (Roth) in PBS and quenching of PFA-induced fluorescence by the addition of 0.12% (w/v) glycine (Roth) in PBS containing 0.2% saponin, the cells were blocked for 1 h with 10% FCS in PBS containing 0.2% saponin. Coverslips were incubated overnight at 4°C with the indicated primary antibodies diluted in PBS containing 0.2% saponin. Fluorophore-conjugated secondary antibodies (Alexa Fluor 488,; Thermo Fisher Scientific) were added for 1 h at room temperature, followed by embedding of the coverslips in 17% (w/v) Mowiol 4–88 mounting solution (Calbiochem) containing 20 mg/mL 1,4-diazabicyclo[2. 2.2]octane (DABCO; Sigma-Aldrich) and 5 μg/mL 4′,6-diamidino-2-phenylindole (DAPI; Sigma-Aldrich) for nuclear staining. Images were analyzed using a Zeiss Axio Observer.Z1/7 Airyscan microscope equipped with a 63× objective. Image acquisition and processing were performed using Zen 3.1 (blue edition) software (Carl Zeiss Microscopy GmbH, Germany).

### Cell- and mouse tissue lysates for immunoblot

Cells (10 cm dish) were lyzed in 100 μL homogenization buffer (50 mM Tris-HCl pH 7.4, 100 mM NaCl, 1% (w/v) Triton X-100, 0.1% (w/v) SDS supplemented with cOmplete Protease Inhibitor (Sigma-Aldrich)) by ultrasonification. Mouse brain lysates were prepared by homogenization of fresh or frozen brain material in a ''Bead Mill 24 Homogenisator'' (Fisher Scientific) in 5 volumes of lysis buffer (50 mM Tris-HCl pH 7.4, 150 mM NaCl, 1% (w/v) Triton X-100, supplemented with cOmplete Protease Inhibitor (Sigma-Aldrich)). After homogenization, the lysates (cells or tissues) were centrifuged for 20 min at 1000 × g at 4°C followed by ultrasonification twice for 20 s at 4°C using a Branson Sonifier 450 (level seven in a cup horn, Emerson Industrial Automation) and lysed on ice for 60 min. The cell lysates were cleared at 16,000 × g for 15 min at 4°C, and the protein concentration of the supernatant was determined using the Pierce BCA (bicinchoninic Acid) Assay kit (Thermo Fisher Scientific) according to the manufacturer's protocol.

### Immunoblot of cell lysates and mouse tissues

Protein lysates were prepared for SDS-PAGE in Lämmli buffer (125 mM Tris/HCl pH 6.8, 10% (v/v) glycerol, 1% (w/v) SDS, 100 mM 1,4-dithiothreitol (Roth) and traces of bromophenol blue) and were denatured for 10 min at 95°C (if not stated otherwise). SDS-PAGE and western blot were carried out according to standard procedures with nitrocellulose membrane (Amersham, Thermo Fisher). After blocking the nitrocellulose membrane with 5% (w/v) skim milk powder in 1x TBS-T buffer for 1 h at room temperature, primary antibodies (diluted in skim milk blocking solution) and the membranes were incubated overnight, followed by washing the membranes and incubation with HRP-coupled secondary antibodies. After washing the membranes in TBS-T buffer, HRP activity was detected using enhanced chemiluminescence (ECL) Ultra (TMA-6) (Lumigen, Michigan, USA) substrate solution and an ImageQuant LAS 4000 (GE Healthcare) imaging device. The intensity of the signal was quantified using ImageJ (Version 1.46r) software. Before incubation with different antibodies, the membranes were stripped using stripping buffer (100 mM glycine (Roth), 20 mM Mg-acetate (Roth), 50 mM KCl (Roth), pH 2.2). Incubation of 30 min at room temperature and gentle shaking was performed in stripping buffer followed by 3 times for 5 min in TBS-T buffer. Next, the membranes were incubated in 5% (w/v) skim milk powder in 1x TBS-T buffer for 1 h at room temperature, followed by incubation with the primary antibody.

### Enrichment of mouse liver lysosomes

The enrichment of lysosomes from the mouse liver was described in detail before.[38]

### Sarkosyl-extraction of fibrils from human brain

To detect full-length TMEM106B (in RIPA-soluble fractions) and TMEM106B fibrils (in sarkosyl-insoluble P3 fractions), human post-mortem frontal cortex tissue was homogenized respectively in 5 volumes (w/v) of ice-cold RIPA buffer (25mM Tris-HCl pH 7.5, 150mM NaCl, 1% Nonidet P-40, 1% sodium deoxycholate, 0.1% SDS, with protease and phosphatase inhibitors) or in 5 volumes (w/v) of cold buffer (10 mM Tris-HCl pH 7.4, 80 mM NaCl, 1 mM $MgCl_2$, 1 mM EGTA, 0.1 mM EDTA, 1 mM PMSF, 1 mM dithiothreitol,

with protease and phosphatase inhibitors). To obtain the RIPA-soluble fractions, supernatants were collected following sonication (1 s on/1 s off for 10 s) and centrifugation at 100,000 x g for 30 min at 4°C. To generate the sarkosyl-insoluble P3 fraction, 400 μL of homogenate was first ultracentrifuged (150,000 × g for 40 min at 4 °C in a TLA110 rotor at 60,000 rpm), and the resulting pellet resuspended in one volume of cold buffer (10 mM Tris pH 7.4, 0.85 M NaCl, 10% sucrose, 1 mM EGTA). After an additional step of centrifugation (14,000 g for 10 min at 16°C), the supernatant was then incubated with sarkosyl (1% for 1 h at room temperature with continuous agitation) and ultracentrifuged (150,000 × g for 40 min at 4 °C in a TLA110 at 60,000 rpm). Finally, 50 μL TE buffer (10 mM Tris-HCl, 1 mM EDTA) was added to resuspend the resulting pellet (sarkosyl-insoluble P3 fraction).

#### *Immunoblot of human brain autopsy material*

RIPA-soluble fraction (20 μg) or sarkosyl-insoluble fraction (10 μL) were diluted with 2× SDS gel loading buffer at a 1:1 ratio (v/v). The RIPA-soluble extracts were maintained on ice without any prior step of denaturation, while the sarkosyl-insoluble P3 fraction was first heated at 95°C for 5 min. Samples were loaded into 20-well 4–20% Tris-glycine gels (Novex) and run on ice. PVDF membranes were used for the transfer and then blocked with 5% nonfat dry milk in TBS plus 0.1% Triton X-(TBS T) for 1 h. Antibody incubation and visualization were performed as described above.

#### *Immunohistochemistry of human brain sections*

Seven micrometers thick sections were deparaffinized in xylene and rehydrated in graded alcohol series. Antigen retrieval was performed by incubating the sections in 80% formic acid for 10 min (for luminal TMEM106B antibodies), followed by boiling in 10 mM Tris/1 mM/EDTA buffer, pH 9.0, in a pressure cooker for 10 min (20 min for E7H7Z). Endogenous peroxidase was quenched with 1% H2O2, and unspecific antibody binding was blocked with 5% bovine serum albumin (30 min RT). Primary antibodies against TMEM106B (luminal domain #118C4, 1:2.000/0.7 μg/mL, rat monoclonal, Cat#506 017, Synaptic Systems, luminal domain TMEM239 1:1.000, rabbit polyclonal, gift from Manuel Schweighauser[18]; or N terminus E7H7Z, 1:200, rabbit monoclonal, 93334, Cell signaling Technology) were incubated overnight at 4°C and visualized with biotinylated anti-rat (1:200, BA-4001, Vector Laboratories) or anti-rabbit (1:200, BA-1100-1.5, Thermo Scientific, for TMEM239 or BA-1000, Vector laboratories, for E7H7Z) secondary antibody and Vectastain Elite ABC Kit Peroxidase (Vector Laboratories) using 3,3′-diaminobenzidine (DAB, Sigma-Aldrich) as chromogen with 5 min incubation time. Sections were counterstained with Mayer's hematoxylin, dehydrated in alcohol series, cleared in xylene, and mounted with DPX (06522, Sigma-Aldrich). Whole section images with 20x (luminal TMEM106B antibodies) and 40x (N-terminal TMEM106B antibody) magnification were obtained with Hamamatsu Nanozoomer XR Digital slide scanner.

## QUANTIFICATION AND STATISTICAL ANALYSIS

GraphPad Prism 9.3.1 (GraphPad Software) was used for data representation and calculation of statistic testing. A two-tailed unpaired t test was used if not indicated otherwise. Statistical differences in the graphs were generally depicted as ns = not significant; *$p \leq 0.05$; ** $\leq 0.01$; ***$p \leq 0.001$; ****$p \leq 0.0001$. Error bars in the graphs represent the standard error of the mean (SEM), as indicated in the figure legends.